

2017

Nonbreaking wave-induced mixing in upper ocean during tropical cyclones using coupled hurricane-ocean-wave modeling

S. Aijaz

M. Ghantous

See next page for additional authors

Follow this and additional works at: <https://digitalcommons.uri.edu/gsofacpubs>

Terms of Use

All rights reserved under copyright.

Citation/Publisher Attribution

Aijaz, S., Ghantous, M., Babanin, A. V., Ginis, I., Thomas, B., and Wake, G. (2017), Nonbreaking wave-induced mixing in upper ocean during tropical cyclones using coupled hurricane-ocean-wave modeling, *J. Geophys. Res. Oceans*, 122, 3939–3963, doi:10.1002/2016JC012219.

Available at: <https://doi.org/10.1002/2016JC012219>

This Article is brought to you for free and open access by the Graduate School of Oceanography at DigitalCommons@URI. It has been accepted for inclusion in Graduate School of Oceanography Faculty Publications by an authorized administrator of DigitalCommons@URI. For more information, please contact digitalcommons@etal.uri.edu.

Authors

S. Ajjaz, M. Ghantous, A V. Babanin, Isaac Ginis, B. Thomas, and G. Wake

RESEARCH ARTICLE

10.1002/2016JC012219

Special Section:

Oceanic Responses and
Feedbacks to Tropical
Cyclones

Key Points:

- Evaluation of nonbreaking wave parameterization in coupled hurricane-ocean-wave model
- Increased SST and enhanced mixed layer depth due to nonbreaking wave turbulence during hurricanes
- Rapid response of increased wave heights to strong winds while delay in maximum SST cooling by a lag of 10–15 h

Correspondence to:

S. Aijaz,
saima.aijaz@bom.gov.au

Citation:

Aijaz, S., M. Ghanous, A. V. Babanin, I. Ginis, B. Thomas, and G. Wake (2017), Nonbreaking wave-induced mixing in upper ocean during tropical cyclones using coupled hurricane-ocean-wave modeling, *J. Geophys. Res. Oceans*, 122, 3939–3963, doi:10.1002/2016JC012219.

Received 6 AUG 2016

Accepted 7 APR 2017

Accepted article online 13 APR 2017

Published online 15 MAY 2017

Nonbreaking wave-induced mixing in upper ocean during tropical cyclones using coupled hurricane-ocean-wave modeling

S. Aijaz¹ , M. Ghanous², A. V. Babanin³ , I. Ginis⁴, B. Thomas⁴, and G. Wake⁵ 

¹Australian Bureau of Meteorology, Melbourne, Victoria, Australia, ²Laboratoire d' Etudes en Géophysique et Océanographie Spatiales, Université de Toulouse, CNES, CNRS, IRD, UPS, France, ³University of Melbourne, Melbourne, Victoria, Australia, ⁴Graduate School of Oceanography, University of Rhode Island, Narragansett, Rhode Island, USA, ⁵Woodside Energy Limited, Perth, Western Australia, Australia

Abstract The effects of turbulence generated by nonbreaking waves have been investigated by testing and evaluating a new nonbreaking wave parameterization in a coupled hurricane-ocean-wave model. The MPI version of the Princeton Ocean Model (POM) with hurricane forcing is coupled with the WAVEWATCH-III (WW3) surface wave model. Hurricane Ivan is chosen as the test case due to its extreme intensity and availability of field data during its passage. The model results are validated against field observations of wave heights and sea surface temperatures (SSTs) from the National Data Buoy Centre (NDBC) during Hurricane Ivan and against limited in situ current and bottom temperature data. A series of numerical experiments is set up to examine the influence of the nonbreaking wave parameterization on the mixing of upper ocean. The SST response from the modeling experiments indicates that the nonbreaking wave-induced mixing leads to significant cooling of the SST and deepening of the mixed layer. It was found that the nondimensional constant b_1 in the nonbreaking wave parameterization has different impacts on the weak and the strong sides of the storm track. A constant value of b_1 leads to improved predictions on the strong side of the storm while a steepness-dependent b_1 provides a better agreement with in situ observations on the weak side. A separate simulation of the intense tropical cyclone Olwyn in north-west Australia revealed the same trend for b_1 on the strong side of the tropical cyclone.

Plain Language Summary Operational and forecast models generally underestimate the intensity of tropical cyclones by underestimating the sea surface temperature and the upper ocean mixing. Although the role of ocean waves is now being regarded as essential in ocean mixing, predictive modeling of tropical cyclones does not always include the effects of turbulence generated by waves that would lead to enhanced mixing and therefore increased cooling of sea surface temperatures leading to improved prediction of tropical cyclone intensity. This paper describes the implementation of a new wave model that simulates the turbulence generated by nonbreaking waves in a coupled ocean-wave-hurricane modeling system.

1. Introduction

Climate and weather including tropical cyclones are essentially air-sea interaction phenomena that involve the coupling of the atmospheric and the ocean physical regimes. The hurricanes gain or lose their strength via the air-sea exchange of heat and moisture while the ocean response is controlled by the momentum exchange [Zweers *et al.*, 2010]. Recent advancements in coupled atmosphere-ocean models have led to significant improvements in the forecast of tropical cyclones. However, the operational atmosphere-ocean models generally do not explicitly include the ocean surface waves, which occur on much smaller scales of both time and space. It is now known that waves influence a great number of processes both in the atmospheric boundary layer and in the upper ocean [Babanin, 2006]. The wave pattern in a tropical cyclone is very complicated and dependent on the intensity, size, and speed of propagation of the cyclone. An average wave field cannot be taken as representative of the wave environment during a cyclone because of the variability of waves in the different quadrants of the cyclone [Young, 1988, 2006]. Therefore, it is necessary

to calculate the wave properties explicitly through each stage of the cyclone development. Recent coupled hurricane-ocean-wave modeling studies [Fan *et al.*, 2009a,2009b; Li *et al.*, 2014; Zambon *et al.*, 2014] have highlighted the significance of the wind-wave-current interactions during tropical cyclones. Accurate prediction of the wave environment in the numerical simulation of tropical cyclones improves the prediction of wind speeds, momentum fluxes, and ocean mixing [Moon *et al.*, 2008]. Coupling air-sea interaction physics with wave dynamics is thus necessary for understanding and modeling of tropical cyclones and climate in general.

Tropical cyclones develop and are maintained by the heat energy that they receive from the ocean. The warmer the sea surface temperature below the cyclone, the higher the energy available to the cyclone. To predict cyclone intensity, we need to know the initial sea surface temperature and the environmental interactions that can heat or cool the ocean surface. Of these mechanisms, the dominant one is the wind forcing that generates strong upper ocean currents and large-amplitude surface waves [Reichl *et al.*, 2016]. The wind-generated currents produce a vertical shear leading to turbulence, which then mixes the upper ocean layer by entraining cooler water from the thermocline up into the well-mixed ocean surface [Yablonsky *et al.*, 2015a] ultimately cooling the SST. Wind-generated waves also create turbulence when they dissipate energy by transferring their momentum to the ocean. Although surface wave-breaking is considered to be responsible for most of the local wave energy dissipation, the turbulent energy it injects into the ocean is confined to a thin surface layer, the scale of which is comparable to the wave heights [Agrawal *et al.*, 1992]. Therefore, the turbulence generated by wave-breaking decays rapidly with distance from the sea surface and is therefore considered as a minor contributor to the overall ocean mixing [Huang *et al.*, 2011].

Another mechanism for production of turbulence by dissipating waves is through the wave-orbital motion of nonbreaking waves. Such turbulence is distributed vertically through the water column at a scale comparable to that of the wave length (wave-orbital motion extends to a depth equal to approximately half the wave length), which is an order of magnitude larger than the wave height [Babanin, 2006]. In finite-depth environments, this turbulence can produce mixing all the way to the seabed in response to a single storm [Babanin and Chalikov, 2012]. This concept has been tested in the field [Pleskachevsky *et al.*, 2011; Toffoli *et al.*, 2012]; in the laboratory [Babanin and Haus, 2009; Dai *et al.*, 2010]; and in multiple numerical experiments [Babanin and Chalikov, 2012; Li *et al.*, 2014; Qiao *et al.*, 2004; Reichl *et al.*, 2016]. Predictions of SST and upper ocean temperature profiles have been shown to improve by up to 35% relative to the observed data when the wave-induced turbulence is included in ocean-circulation and general-circulation models, depending on wave climate at a particular location and on latitude [Qiao *et al.*, 2010; Huang *et al.*, 2008].

The wave-induced mixing in numerical models has been parameterized previously using several approaches. Qiao *et al.* [2004] developed a parameterization for wave mixing induced by the wave-orbital motion, in which a new mixing term, B_v , represented the wave-induced turbulent viscosity. This has been applied to a three-dimensional ocean-circulation model, the POM [Blumberg and Mellor, 1987] by adding it directly to the turbulent viscosity in the two-equation Mellor-Yamada turbulence model, and to the turbulent viscosity in the K Profile Parameterisation (KPP) model [Wang *et al.*, 2010] and other ocean general-circulation [Shu *et al.*, 2011] and climate models [Huang *et al.*, 2008; Huang and Qiao, 2010]. The KPP and the Mellor-Yamada turbulence models are calibrated empirically; therefore, any addition of new data would require recalibration. Although the inclusion of B_v in both models lead to a more accurate prediction of ocean mixing in the presence of waves, it does not appear that the turbulent models had been recalibrated in these studies.

Other parameterizations of wave-induced turbulence include those that are scaled against the wind stress [Jacobs, 1978; Huang and Qiao, 2010] or those with Langmuir circulation, which may not always be present. Kantha and Clayson [2004] have parameterized Langmuir circulation by adding Stokes shear to the current shear in the turbulence production terms in the Mellor-Yamada turbulence model. Reichl *et al.* [2016] have recently modified the KPP model to include the effects of enhanced turbulence generated by Langmuir circulations. Their procedure consists of applying a separate enhancement factor to each contribution to the mixing coefficients and the turbulent shear terms to account for the different length and velocity scales associated with them.

The wave-induced mixing can change the SST in the course of a tropical cyclone's development [Wang and Qiao, 2008]. Since the cyclone intensity relies on SST as a primary source of energy, such mixing can affect

its intensity or even its tracking. Improvements in wave mixing physics in numerical models would thus contribute to improvements of predictions and forecast guidance of tropical cyclones. The objectives of this study are to describe the implementation and validation of the nonbreaking wave parameterization of *Ghantous and Babanin* [2014a,2014b] in a three-dimensional coupled hurricane-ocean-wave model. This validation has not been undertaken yet in terms of mixing with the only other study being *Walsh et al.* [2015], and that is at the climate scale. The wave parameterization defines the nonbreaking wave turbulence produced by the wave-orbital motion (or already existing and fed from the orbital motion). Hurricane Ivan has been chosen as a test case because of its extreme intensity and the availability of wave and ocean data from permanent buoys deployed in the Gulf of Mexico. Hurricane Ivan has been the subject of several investigations [*Fan et al.*, 2009b; *Halliwel et al.*, 2011; *Zambon et al.*, 2014], and these provide valuable information for comparison with the present study.

The paper is organized as follows: the wave parameterization is discussed in section 2. The coupled models and the detailed model setup are described in section 3; the model results and their discussion are presented in section 4 and the conclusions are summarized in section 5.

2. Nonbreaking Wave-Induced Parameterization

The nonbreaking wave-induced parameterization tested in this study is based on a set of laboratory experiments by *Babanin and Haus* [2009] where the dissipation of turbulent kinetic energy near the surface was measured during the passage of waves. A relationship for the volumetric dissipation of turbulent kinetic energy was determined. Assuming a steady state where the rate of dissipation of turbulent kinetic energy is equal to its rate of production, and further assuming that all energy dissipated by nonbreaking waves goes into turbulence production, the turbulence production P_w is then given by [*Ghantous and Babanin*, 2014a,2014b]

$$P_w = b_1 k \omega^3 \frac{H^3}{8} e^{3kz} \tag{1}$$

where H is the wave height; z is the water depth (positive upwards); k is the wave number; ω is the radian frequency; and b_1 is a nondimensional proportionality constant. *Young et al.* [2013] found a value of 0.0014 for b_1 by analysing the rate of swell attenuation from altimeter observations in the Great Australian Bight. This value of b_1 represents an upper bound of the best fit to the altimeter data based on an analytical solution of (1). The study acknowledges that swell attenuation may not be a true measure of swell energy dissipation; however, it is known that it is difficult to separate all active processes from the altimeter data [*Zieger et al.*, 2015].

Arduin et al. [2010] have proposed a dynamic value for b_1 derived from the synthetic aperture radar observations [*Arduin et al.*, 2009]. Using the same radar observations, *Babanin* [2011] compared the swell dissipation rates of *Arduin et al.* [2009] with a depth-integrated form for the turbulence dissipation and estimated b_1 as 0.002. The data were also found to exhibit a quadratic dependence on wave steepness, thus b_1 was calculated as

$$b_1 = 5 \left(\frac{H}{2} k \right)^2 \tag{2}$$

where $\left(\frac{H}{2}k\right)$ is the wave steepness. *Ghantous and Babanin* [2014b] found that when compared to laboratory measurements, (2) produced too much mixing. This was attributed to (a) the absence of turbulence when the water in the laboratory tests was left to rest; (b) the assumption that orbital motion is the only source of dissipation; and (c) approximations in the application of monochromatic waves. Recently, *Zieger et al.* [2015] have demonstrated that applying a linear dependence of steepness to b_1 leads to a considerable improvement in the mean bias of modeled wave heights in a global hindcast when compared to altimeter data. Their formula for b_1 is

$$b_1 = B_1 2Ek_p \tag{3}$$

where B_1 is a scaling coefficient; E is the total sea surface variance; and k_p is the peak wave number.

We conducted modeling tests using constant $b_1 = 0.0014$, and b_1 using (2) and (3) under hurricane conditions. We found that the magnitude of b_1 resulting from (3) is at least 2 orders of magnitude less than that

of $b_1 = 0.0014$. It is also significantly smaller than the b_1 computed from (2). Moreover it leads to SST values that are nearly similar when $b_1 = 0$ (i.e., when there is no wave-induced mixing). In view of above, we excluded b_1 from (3) from further detailed analyses.

There are two main mechanisms for the wave-orbital-induced turbulence in (1): first, via the shear stresses when the viscosity of water is taken into account [Phillips, 1961]; second, the instability of three-dimensional (3-D) vorticity due to the wave orbits, even if the latter are regarded potential [Benilov, 2012]. The latter mechanism is based on a strict mathematical theory, which is valid if the turbulence is preexisting. As the ocean is nearly always turbulent, in principle the theory is considered generally applicable to ocean wave turbulence regardless of the exact source of turbulence. Other sources of wave turbulence can include interactions of background turbulence with Stokes current and Langmuir turbulence. Our study does not explicitly include these two sources. It is an open question as to whether Langmuir circulation can be considered to be an implicit part of (1) since it is driven by the Stokes drift, which is a property of the wave-orbital motion. In any case, the nonbreaking wave-induced mixing extends to deeper ocean layers (depths up to half the wavelength) and should in principle always feature when waves are present, whereas Langmuir cells do not. Because of this, and because there is no clear reason why having both would necessarily produce more useful results, we do not include a separate Langmuir parameterization. More on this may be found in the brief discussion in Ghantous and Babanin [2014a, section 6].

The main advantages of the nonbreaking wave parameterization described in (1) are that it is independent from the wind stress, and therefore does not rely on wave-breaking; it employs a characteristic length scale (radius of the wave orbit) as opposed to the law of the wall turbulence which does not have a characteristic length other than distance to the surface [Babanin, 2011]; it allows the turbulence model to respond to stratification by virtue of the fact that it is added to the turbulence production before a turbulent viscosity is calculated; and can be easily adapted into viscous turbulence models without the issues sometimes encountered in some methods of trying to add together generally nonadditive viscosities.

3. Coupled Hurricane-Ocean-Wave Model Setup

The new Message Passing Interface (MPI) version of the POM for tropical cyclones (MPIPOM-TC) coupled with the WAVEWATCH III (WW3) wave model [Tolman, 2009] was used for the coupled ocean-wave-hurricane modeling. The new MPIPOM-TC consists of flexible initialization options for hurricane simulations and allows for relocatable grids around the globe [Yablonsky *et al.*, 2015b]. The MPIPOM-TC code is a modified version of the original POM [Blumberg and Mellor, 1987; Mellor, 2004] adapted to run in parallel on a distributed memory computer. The MPIPOM-TC model has been successfully coupled to the Geophysical Fluid Dynamics Laboratory (GFDL) hurricane model and to the atmospheric component of the Hurricane Weather Research and Forecast (HWRF) Model at NOAA [Yablonsky *et al.*, 2015b].

A dynamic coupler has been developed at the University of Rhode Island specifically for the coupling of MPIPOM-TC with the surface wave model, WW3. The atmospheric model passes the winds to both the wave and the ocean models. The wave model simulates the wave fields and then passes the wave parameters to the ocean model where they are used to compute the wave-induced mixing in the ocean model, which in turn impact the currents and the overall mixing.

3.1. The Atmosphere/Hurricane Model, TC

The wind fields for the coupled hurricane model are generated by a prescribed hurricane wind forcing or two-way coupling between the ocean and a prognostic hurricane model such as HWRF or GFDL [Yablonsky *et al.*, 2015b]. In this study, we use prescribed winds to calculate the surface wind forcing using observations along the storm track. These observations, known as the TC (tropical cyclone) vitals, are based on the National Hurricane Centre (NHC), Joint Typhoon Warning Center (JTWC); Australian Bureau of Meteorology (BoM) database; or other similar databases, and consist of the TC position, propagation speed and direction, central and environmental pressure, radius of outermost closed isobar, maximum wind speed, radius of maximum wind, and radii of 18 and 26 m/s winds in the northeast, southeast, southwest, and northwest quadrants. Each of these parameters is linearly interpolated in time so as to generate a coherent storm

structure at all model time steps [Buetti *et al.*, 2014]. An empirical wind field is calculated based on the radii of the 18 and 26 m/s winds in each quadrant of the storm when available from the TC vitals database. For each location in space, the radial distance from the storm center and the angle from north are calculated. The resulting tangential and radial components of the wind speed are then converted into zonal and meridional components. If detailed structure of the storm from the TC Vitals database is unavailable, then the axisymmetric wind profile of Holland [1980] and Holland *et al.* [2010] is used. Finally, the hurricane model interpolates the winds profiles on the ocean (MPIPOM-TC) and the wave (WW3) model grids.

3.2. The Ocean Model, MPIPOM-TC

The ocean model component MPIPOM-TC is a three-dimensional, free surface, terrain-following numerical model that solves the Navier-Stokes equations using the hydrostatic and Boussinesq assumptions. The density field is determined from the UNESCO equation of state that accounts for pressure, potential temperature, and salinity.

MPIPOM-TC has a relocatable grid such that the model domains have a worldwide coverage [Yablonsky *et al.*, 2015b]. Each of the eight [8] region-specific domains are set to the same size: 869×449 (longitudinal \times latitudinal) grid points, covering 83.2° and 37.5° of longitude and latitude intervals respectively, yielding a horizontal grid spacing of ~ 9 km. The horizontal domain decomposition is 3×3 , with 291 grid points along the longitude and 151 local grid points along the latitude on each of nine (9) processors. The two grids used in the study are the "Transatlantic" grid and the "Southwest Pacific" grid. The Transatlantic grid (Figure 1) bounds a region in the North Atlantic from 10°N to the south and 47.5°N to the north, and from 98.5°W to the west and 15°W to the east. The model domain for the Southwest Pacific grid is set at 40°S – 2.5°S latitude and 96.5°E – 178°E longitude. A 5 arc min global model of the Earth's topography and bathymetry [ETOPO5, 1988] is used to define the seabed. The minimum depth is set as 10 m.

The horizontal MPIPOM-TC grid uses curvilinear orthogonal coordinates, and an Arakawa C differencing scheme [Mellor, 2004]. The horizontal time differencing is explicit, but vertical time differencing is implicit. There are 23 full sigma levels from the sea surface to the seabed, with higher vertical resolution in the mixed layer and upper thermocline. MPIPOM has a free surface and a split time step [Yablonsky *et al.*, 2015b], the external mode is two-dimensional (2-D) with a time step of 6 s, while the internal mode is 3-D and uses a longer time step of 4.5 min.

The vertical mixing coefficients in the ocean model are computed by the Mellor-Yamada level 2.5 turbulence closure model [Mellor and Yamada, 1982; Mellor, 2004]. This turbulence scheme is based on approximations to the equations for turbulent kinetic energy and Reynolds stresses by Rotta and Kolmogorov, which have been extended to stratified flow cases [Mellor, 2004]. It requires specification of six empirical constants. The constants are based on observations in which the shear production is balanced by the dissipation. Although the shear production and dissipation may not balance in the presence of breaking waves, Craig and Banner [1994] have shown that the level 2.5 scheme works well in the wave-affected surface layer of the ocean when the waves are breaking. The Smagorinsky diffusivity is used for horizontal diffusion. The

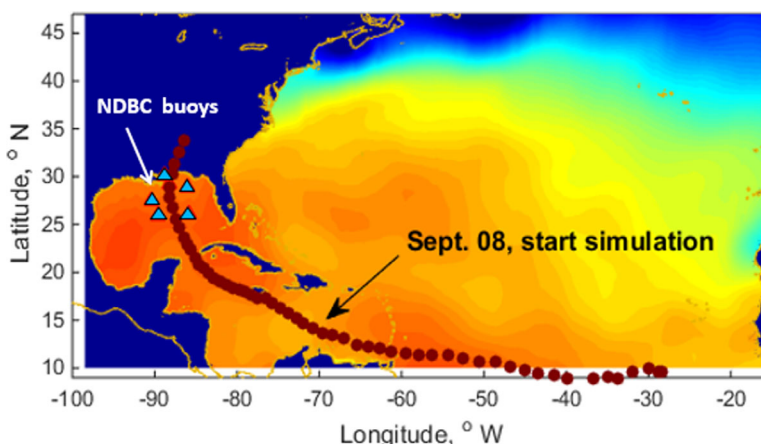


Figure 1. Model extent; NDBC buoys (triangles); and Hurricane Ivan best track (dark circles).

coefficients for vertical eddy viscosity and diffusivity are estimated as $K_M = qS_M$, and $K_S = qS_H$, where $q^2/2$ is the turbulent kinetic energy (TKE); S_M and S_H are dimensionless stability functions; q the turbulent velocity scale; and l the macro length scale of turbulence. The quantities q and l are modeled by means of the Mellor-Yamada two-equation model. The nonbreaking wave-induced parameterization P_w from (4) is added to both the Mellor-Yamada transport equations. The two transport equations, first one for TKE $q^2/2$ and the second for the quantity q^2l are

First equation

$$\partial t \left(\frac{q^2}{2} \right) - \partial z \left[qS_q \partial z \left(\frac{q^2}{2} \right) \right] = P_s + P_b + P_w - \varepsilon \tag{4}$$

Second equation

$$\partial t (q^2l) - \partial z (qS_q \partial z (q^2l)) = l \left\{ E_1(P_s + P_w) + E_3P_b - \left[1 + E_2 \left(\frac{l^2}{L} \right) \varepsilon \right] \right\} \tag{5}$$

where $P_s = K_M S^2$ is the shear production; $P_b = K_H N^2$ is buoyancy production; S is the shear frequency; N is the Brunt-Väisälä frequency; ε is the dissipation rate of TKE; E_1 , E_2 , and E_3 , S_q are constants; and L is the empirical nonlocal length scale. The turbulent dissipation terms in both the q^2 and q^2l equations are discretized in time in MPIPOM-TC. The turbulent production terms involve estimates of the square of the vertical shear in the horizontal velocity and the vertical potential density gradient.

The ocean model in MPIPOM-TC is forced by the wind stress, and the wind-generated ocean currents are then modified by growing or decaying wave fields, and the overall mixing is enhanced by the new non-breaking wave-induced turbulence.

We have disabled the modified form of the surface wave-breaking parameterization of *Craig and Banner* [1994] (CB) in the ocean model (MPIPOM-TC) to avoid any potential conflict in applying two different parameterizations to define the same physical process of turbulence production. The CB model adds a flux of turbulent kinetic energy by modeling the wave-breaking as a surface diffusion boundary condition. Although this condition was not expected to affect the boundary layer deepening, it was found that it results in the deepening of the boundary layer and subsequent cooling of surface temperature [Mellor and Blumberg, 2004]. The layer of enhanced dissipation due to surface wave-breaking has a thickness that is of the order of the magnitude of wave heights [Melville, 1994], which is much less than that of the wave lengths. Any depth penetration of turbulence would be strongly affected by wave-orbital motions [Thomson et al., 2016] that scale with the wave length and not the wave heights. The nonbreaking wave-induced parameterization defines the injection of wave turbulence below the surface due to wave-orbital motions that scales with the wave lengths. On this basis, we have excluded the CB model in MPIPOM-TC. It should be noted that the dissipation produced by the surface wave-breaking is explicitly modeled by the wave model (WAVEWATCH III) and is included in our simulations where the wave model has been coupled with the ocean model MPIPOM-TC.

3.3. The Wave Model, WAVEWATCH III (WW3)

Although newer versions of WW3 (version 4 and above) were available at the time of our study, we chose version 3.14 mainly because it contains the modified drag parameterization that has been shown to be more consistent with field and laboratory observations of the drag coefficient [Donelan et al., 2004; Powell et al., 2003] than the drag coefficient used by the NCEP WW3 model. The original drag coefficient used in WW3 greatly overestimates the wind stress for high wind speeds [Powell et al., 2003; Moon et al., 2007] and results in unrealistic vertical mixing. Therefore, for wind speeds exceeding 12.5 m/s, the WW3 drag parameterization in WW3 has been replaced by the formulation of Moon et al. [2004a, 2004b], which has been derived empirically using coupled wind-wave simulations in hurricanes. The modified drag coefficient has further resulted in more accurate simulations of wave conditions during Hurricane Katrina [Moon et al., 2008] and Hurricane Ivan [Fan et al., 2009b] when compared against buoy measurements.

The wind input function in WW3 represents the energy or the momentum flux transferred from the wind to the waves. Several studies [Janssen, 1989; Chalikov and Makin, 1991] have reported that the momentum flux

(total stress) is the contribution of wave fluctuations and turbulent fluctuations. Near the surface, the total stress consists of contributions due to the wave-induced stress, turbulent stress, and the viscous stress.

The ocean currents passed from MIPOM-TC to the wave model affect the wave fields through the wind input term in the calculation of the wind stress and through the modulation of the wave spectrum by the ocean currents [Fan et al., 2009a]. The evolution of the wave spectrum in WW3 is described by means of the wave action balance equation, which can be written as

$$\frac{\partial N}{\partial t} + \nabla_x \cdot [U_c + c_g]N - \frac{\partial}{\partial k} \left[k \cdot \frac{\partial U_c}{\partial s} N \right] + \frac{\partial}{\partial \theta} \left[\frac{1}{k} \cdot \frac{\partial U_c}{\partial m} N \right] = \frac{S_{tot}}{\sigma} \quad (6)$$

where $N = F(k, \theta, x, t)/\sigma$ is the wave action density spectrum dependent on angular frequency $\sigma = 2\pi f$ from a frame of reference relative to the local currents, wave direction θ ; distance vector x , and time t ; f is the frequency; c_g is the group velocity; U_c is the ocean current; k is the wave number vector; s is the coordinate in the wave direction; and m is the coordinate perpendicular to s . The variable ocean current U_c modifies the speed of the wave action flux and the wave number of the wave packet as it propagates [Fan et al., 2009b]. The term on the right-hand side S_{tot} represents all energy fluxes contributing to wind-wave evolution; and the action density is related to the energy density as simply $N = E/\sigma$. In deep water, it is generally accepted that wind-wave growth is primarily a result of three physical processes: atmospheric input from the wind to the waves; wave dissipation (resulting from breaking and interaction with turbulence and viscosity); and nonlinear energy transfer between the wave components. In finite-depths, additional terms resulting from the bottom friction; depth-induced breaking; and triad interactions may become significant.

The wave spectrum in WW3 for this study has been discretized into 24 directions and 40 frequencies in the range 0.0285–1.1726 Hz with a logarithmic increment $f_{n+1} = 1.1f_n$. The ST2 physics for the source terms [Tolman and Chalikov, 1996] and a modified drag parameterization in WW3 empirically derived from coupled wind-wave simulations in hurricanes have been adopted.

The wave model passes variables for significant wave height, mean wave length, bottom orbital velocity, and the wave radiation stress gradient to the ocean model. The bulk fluxes of surface stresses are then computed and used by MIPOM-TC. The sea surface height and the currents are passed from MIPOM-TC to WW3.

3.4. Model Initialization

Model initialization along with accurate locations of ocean currents and eddies and representative temperature and salinity profiles, is the most important factor to achieve good model performance in comparison with model resolution, and other factors such as ocean dynamics and mixing parameterizations [Halliwell et al., 2011]. The ocean model in the present study is initialized using the feature-based modeling procedure developed by Yablonsky and Ginis [2008]. Historical and near-real-time observations of major ocean fronts are incorporated to account for spatial and temporal variability of mesoscale oceanic features in the Gulf of Mexico, including the Loop current, warm-core rings and cold-core rings.

The initialization of the ocean model consists of three steps [Yablonsky et al., 2015a]:

1. The “diagnostic integration” wherein MIPOM-TC is initialized with realistic 3-D temperature and salinity fields taken from the Generalized Digital Environmental Model (GDEM) monthly ocean temperature and salinity climatology [Teague et al., 1990], which has $1/2^\circ$ horizontal grid spacing and 33 vertical levels. The GDEM climate data are then modified by interpolating in time to the MIPOM-TC initialization date (using 2 months of GDEM), incorporating a land–sea mask, bathymetry data, and the observed structure of the ocean fronts and eddies. Real-time daily SST data (1° grid spacing) is assimilated and the 3-D salinity and temperature profiles are then interpolated from the GDEM levels on to the MIPOM-TC vertical sigma levels. For the Southern Hemisphere, the feature-based modeling procedure has not been used. Although there are no significant large-scale eddies in this model domain, there is a major ocean current, which for the preliminary testing has not been considered.
2. The 48 h “phase 1 spin-up” consists of the dynamic adjustment of density fields and generation of ocean currents. During this phase, SST is held constant.

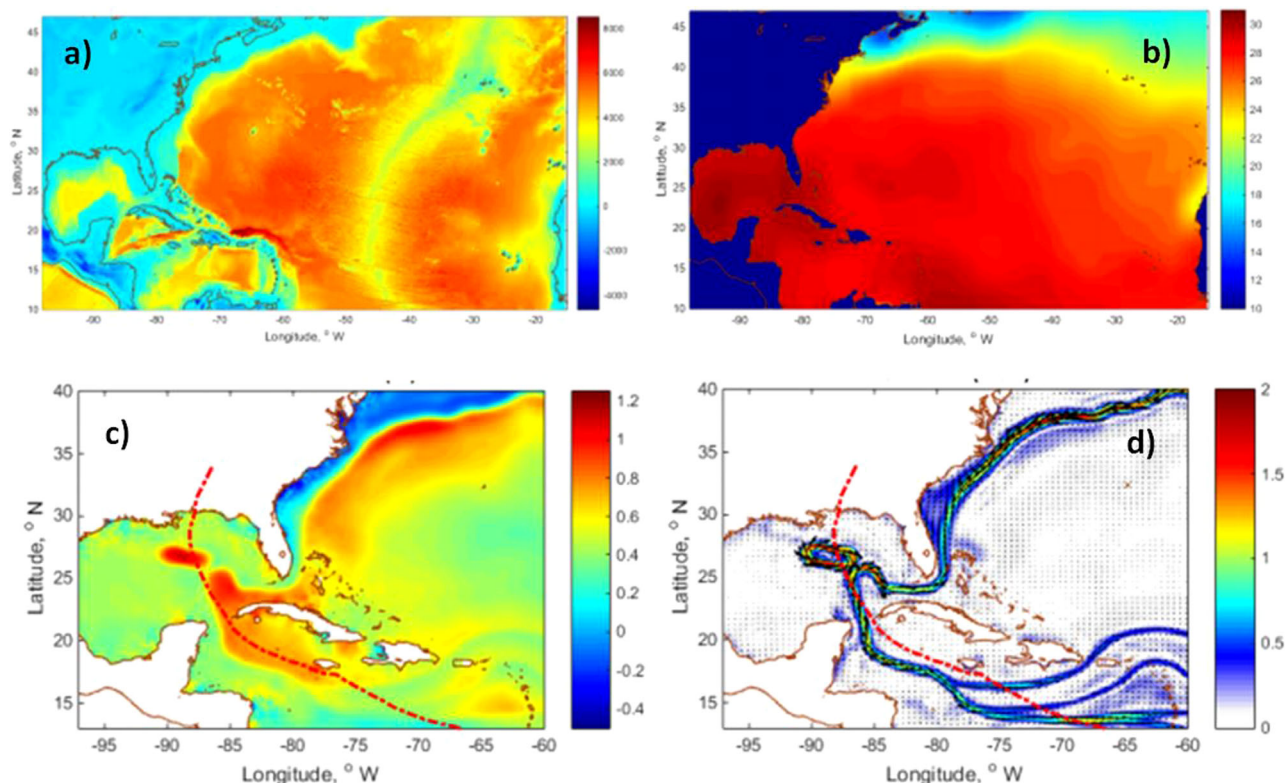


Figure 2. Initial conditions on 8 September 2004 for model input: (a) bathymetry; (b) SST; (c) sea surface elevation; and (d) current velocity vectors and current magnitude (contours).

- The phase 1 output initiates the 72 h “phase 2 spin-up” in which the cold wake at the ocean surface and the currents are generated using the observed hurricane surface winds from the TC vitals provided by NOAA’s National Hurricane Centre.

The output from phase 2 is used to initialize the coupled MIPOM-TC. The wave model is started from calm conditions. Figure 2 shows the initial conditions for the ocean model.

Air temperature, humidity, precipitation, cloud cover, heat flux, and short-wave radiation fluxes have not been included as model inputs for the present study. However, employing direct observations of ocean surface temperatures and other climatology as model inputs in the model initialization precludes the need for air temperature and cloud cover.

3.5. Model Simulations: Hurricane Ivan

To represent 3-D real-world simulations, Hurricane Ivan has been chosen to assess the coupled MIPOM-TC-WW3 model system consisting of the nonbreaking wave parameterization. Hurricane Ivan was an intense long-lived hurricane that reached the Saffir-Simpson category 5 (winds greater than 70 m/s) three times as it moved through the Caribbean Sea and into the Gulf of Mexico in September 2004. It made two landfalls and caused extensive damage to the offshore oil and gas industry in the Gulf of Mexico. Hurricane Ivan intensified into a category 1 hurricane on 5 September 2004 in the North Atlantic Ocean near 9.7°N, 44.3°W. It entered the Caribbean Sea on 8 September 2004 and intensified to category 4, and continued to move northwest entering the Gulf of Mexico on 14 September 2004 as it intensified to category 5 [Teague *et al.*, 2007]. The present study focuses on its development from 8 September 2004 to 17 September 2004 immediately prior to its first landfall on 17 September 2004, west of the Gulf Shores in Alabama. The six buoys from the NOAA NDBC located within 4° of the hurricane track recorded wave parameters and SST during the passage of Hurricane Ivan (Figure 1). The data from the buoys have been mainly used to validate the model results. In addition, the model was compared with limited in situ current and temperature data reported in Teague *et al.* [2007].

Table 1. Numerical Experiments Designed to Evaluate Impacts on Vertical Mixing

Model Run	Processes Included	Processes Excluded
M1	1. Advection, horizontal diffusion, pressure gradients, Coriolis, temperature flux, salinity flux	1. Vertical mixing due to wind stress [surface momentum fluxes $\ll 0.1$] 2. Vertical shear turbulence; $q^2 \ll 0.1$ in [4] and [5] 3. Nonbreaking wave turbulence; $P_w = 0$ in [4] and [5] 4. Dynamic coupling of MPIPOM-TC and WW3; $F = 0$ in [6]
M2	1. Same as M1 2. Vertical shear turbulence from [4] and [5]	1. Vertical mixing due to wind stress [surface momentum fluxes $\ll 0.1$] 2. Nonbreaking wave turbulence; $P_w = 0$ in [4] and [5] 3. Dynamic coupling of MPIPOM-TC and WW3; $F = 0$ in [6]
M3	1. Same as M1 2. Vertical shear turbulence from [4] and [5] 3. Surface wind stress	1. Nonbreaking wave turbulence; $P_w = 0$ in [4] and [5] 2. Dynamic coupling of MPIPOM-TC and WW3; $F = 0$ in [6]
M4	1. Same as M1 2. Vertical shear turbulence from [4] and [5] 3. Surface wind stress 4. Nonbreaking wave turbulence due to spatially and temporally uniform waves; $P_w \neq 0$ in [4] and [5] and $b_1 = 0.0014$ in [1]	1. Dynamic coupling of MPIPOM-TC and WW3; $F = 0$ in [6]
M5	1. Same as M1 2. Vertical shear turbulence from [4] and [5] 3. Surface wind stress 4. Dynamic coupling of MPIPOM-TC and WW3	1. Nonbreaking wave turbulence; $P_w = 0$ in [4] and [5]
M6	1. Same as M1 2. Vertical shear turbulence from [4] and [5] 3. Surface wind stress 4. Nonbreaking wave turbulence; $P_w \neq 0$ in [4] and [5]; $b_1 = 0.0014$ in [1] 5. Dynamic coupling of MPIPOM-TC with WW3	
M7	1. Same as M1 2. Vertical shear turbulence from [4] and [5] 3. Surface wind stress 4. Nonbreaking wave turbulence; $P_w \neq 0$ in [4] and [5]; b_1 from [2] 5. Dynamic coupling of MPIPOM-TC with WW3	

We undertook a number of numerical experiments (Table 1) to determine the effects of wave-induced mixing on the SST and on the overall mixing of the upper ocean layers. We initially started with systematically excluding all vertical mixing (M1), then gradually added the vertical mixing due to shear (current) turbulent kinetic energy (M2); wind stress (M3); nonbreaking wave-induced mixing with uniform (spatially and temporally) wave conditions (M4); vertical shear turbulence with spatially varying wave fields (M5); and nonbreaking wave-induced mixing with spatially varying wave fields with two different b_1 (M6 and M7).

4. Results and Discussion

4.1. Model Validation

To assess MPIPOM-TC-WW3, observations from the NDBC are compared with the simulated significant wave heights (H_s) and SST, shown in Figures 3 and 4, respectively. The validation exercise has been undertaken using Model Run, M6 that includes dynamical coupling of MPIPOM-TC (ocean model) with WW3 (wave model) and P_w (nonbreaking wave-induced parameterization from (1)) (see Table 1). The modeled data from nearby grid points are also shown (in grey) in addition to the data extracted from the closest grid point to indicate any errors due to insufficient horizontal model resolution. Overall, the H_s from the WW3 simulations and the SST from MPIPOM-TC show reasonable agreement with the observations. Data from the NDBC 42040 are missing after 16 September 2004 as the buoy was adrift after this date.

The model shows greater skill in predicting H_s at locations 42039, 42040, and 42041 than at the other sites. It tends to overestimate the H_s at buoy 42003 and underestimate it at 42007. There is a 3–6 h phase lag between the modeled and observed H_s at buoys 42001 and 42003. The discrepancies between the model and the observations may be attributed to inaccuracies in the storm propagation speed and inaccuracies in the interpolation of the prescribed winds generated from the best track data. A similar phase lag between

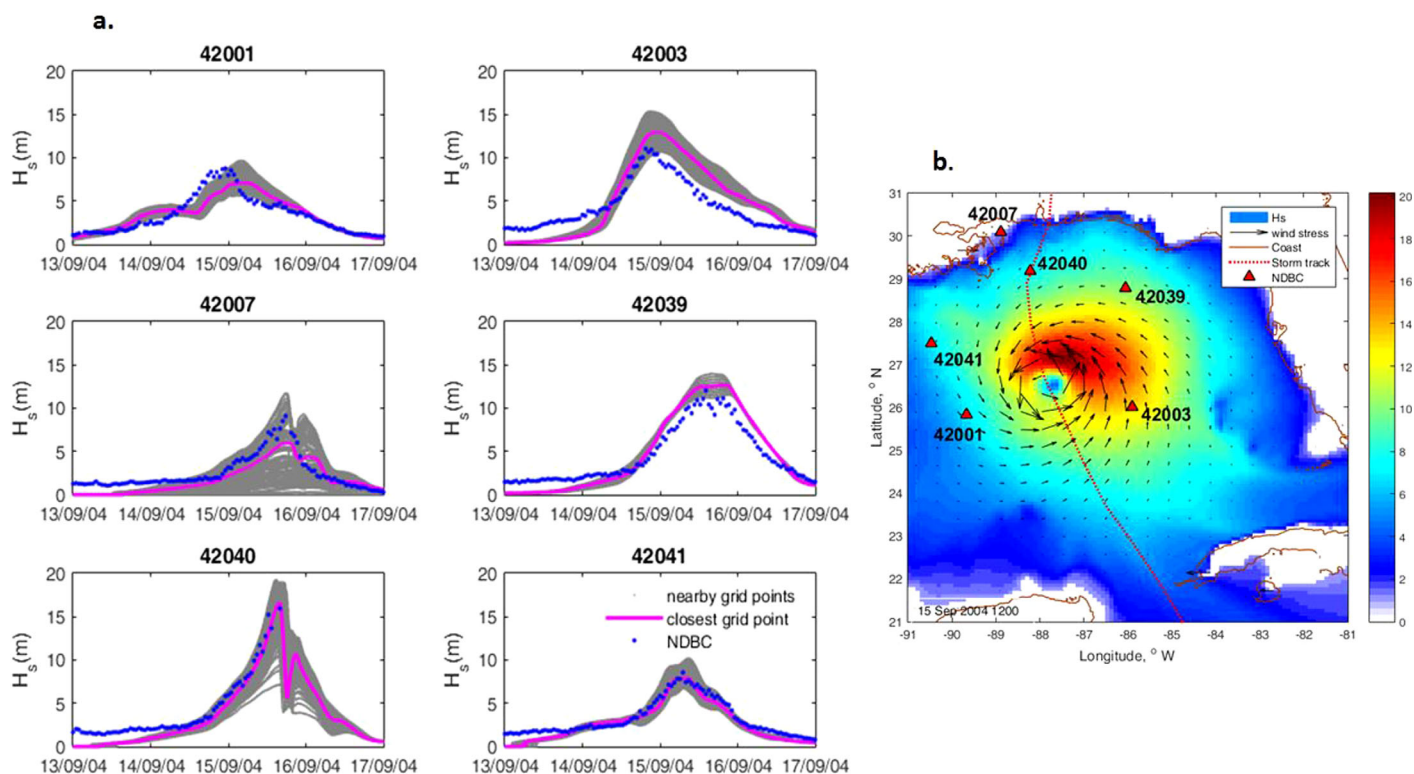


Figure 3. (a) Comparison of modeled significant wave heights (H_s) with observed significant wave heights from the NDBC. The grey lines depict model data from nearby grid points while the pink line represents model data from the closest grid point to the buoy location. (b) Model wind stress vectors, model H_s contours, and NDBC buoy locations for data extracted on 15 September 2004 1200 (Model Run M6).

the model H_s and the H_s at buoy 42001 is seen in the coupled ocean-wave modeling results of Hurricane Ivan undertaken by *Fan et al.* [2009b]. Although our model setup corresponds to Exp. C of *Fan et al.* [2009b], the H_s from our model (Figure 3a) compares more favorably with Exp. A of *Fan et al.* [2009b] that does not include currents or the modified drag parameterization. It is speculated that the primary reason for this discrepancy may be the variation in wind fields between the two model setups. The present study utilizes synthetic winds generated from the TC vitals in the NHC best track while *Fan et al.* [2009b] obtained wind fields from NOAA/HRD real-time wind analysis. The surface wave field is complex and fast—varying in space and time in response to the hurricane conditions and significantly affects the fluxes at the air-sea interface, which are then exchanged between the atmosphere, ocean and the wave models. Additional differences between the two models may be attributed due to the inclusion of the wave-induced mixing parameterization (in the present study), differing model resolution, and the dynamics of the atmosphere-ocean-wave model coupling.

Similar to *Fan et al.* [2009b] and *Zambon et al.* [2014], we see a significant departure of the modeled H_s from the observed H_s at buoy 42007 in our modeling study. This is to be expected because the buoy is located in shallow water (12 m). Consequently, the waves at this location will be subject to nearshore effects, which the model may not capture with good accuracy. The model bathymetry in shallow water is not likely resolved sufficiently by the 9 km horizontal grid resolution. Being close to the coastline, the depths can vary widely in the vicinity of this location. This is evident from the wide range of modeled H_s at grid points near buoy 42007 caused by sharp gradients in depths.

Figure 3b shows that the maximum H_s exceeds 20 m within the hurricane core where the wind stress is strongest in the front right quadrant of the hurricane. The buoys 42001, 42003, and 42041 are located within the warm-core rings of the Loop current and the strong wave-current interactions at these locations will have a strong influence on model performance. This is further discussed in section 4.2.

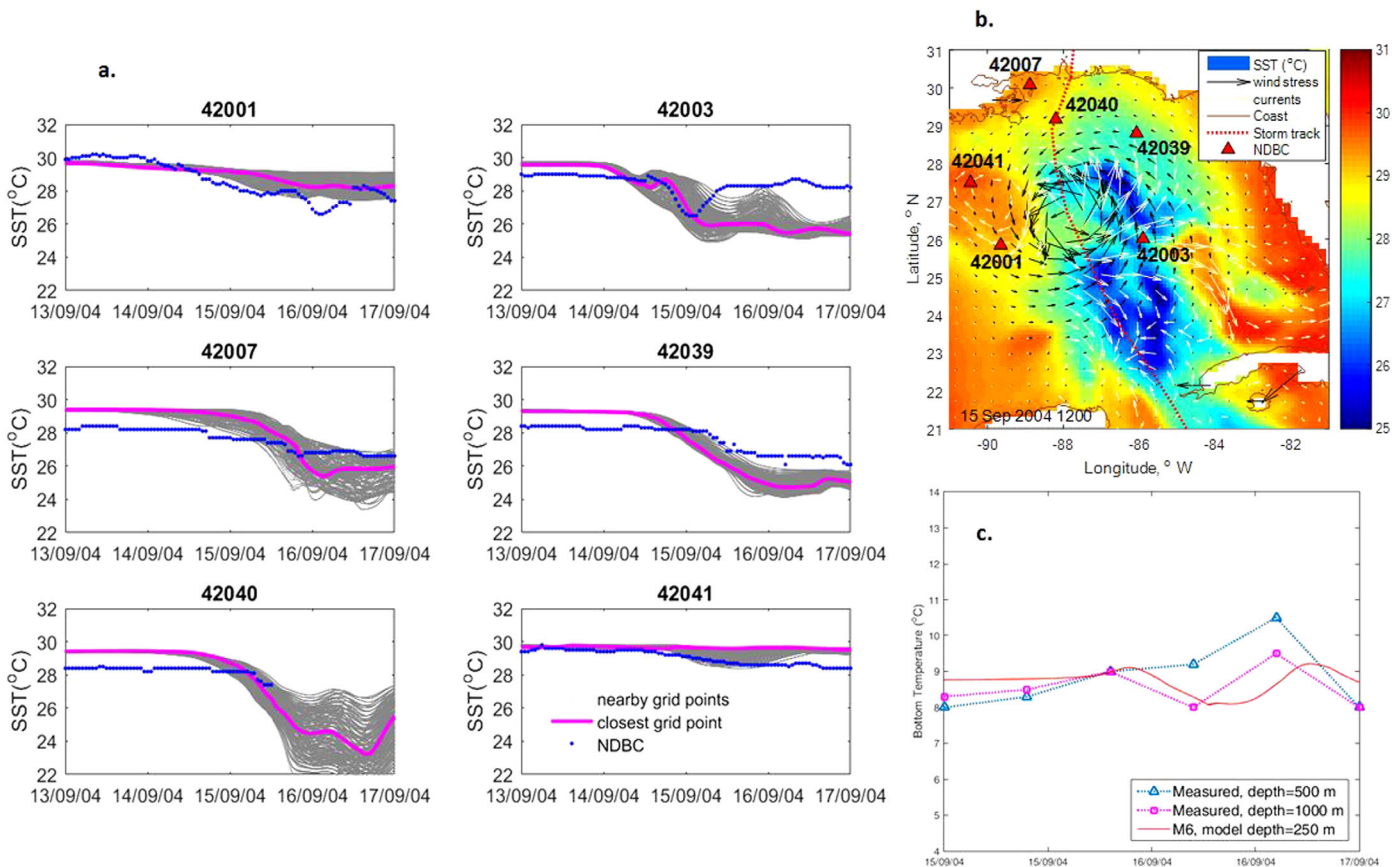


Figure 4. (a) Comparison of modeled sea surface temperature (Model Run M6) with observed sea surface temperature from the NDBC. The grey lines depict data from nearby grid points while the pink line represents data from the closest grid point to the buoy location. (b) Model wind stress vectors (black), model current vectors (white) for M7 on 15 September 2004 1200, model Hs contours, and NDBC buoy locations. Red dotted line is the Hurricane Ivan track. (c) Measured [from *Teague et al., 2007*] and modeled bottom temperature at location 42040.

Figure 4a presents the time series of the observed and modeled SST for M6; this experiment includes dynamic ocean-wave coupling and the nonbreaking wave parameterization. The SST results for all experiments M1–M7 are shown in Figure 5a. In contrast with H_s (Figure 3a), which is affected by water depths comparable to its magnitude, the SST is influenced by the mixed layer water depth, which can extend to 100–200 m during intense storms. Therefore, we see large variations in the modeled SST not only at nearby grid points around the shallow water location of buoy 42007 but also at locations 42039 and 42040, where the water depths are 264 and 165 m respectively. Interestingly, location 42003 in water depth of approximately 3200 m also shows a large variation. At locations away from the eyewall of the TC, the modeled wind speeds are significantly lower leading to less mixing. This large variability in wind speeds causes large variability in SST model predictions in nearby grid points. The large variation in SST is also likely due to the presence of the strong eastward flowing current of the warm-core ring immediately south of buoy 42003. The grid points located within the warm-core ring show SSTs that are 2–3°C higher than the SST at points located above the warm-core ring (Figure 4b). The largest range of SST (exceeding 5°C) is seen at buoy 42040 (Figure 4a). This buoy not only is located in a water depth of less than 200 m but also lies directly in the path of the hurricane track where sea surface cooling is the most intense. With the passage of the hurricane, there is intensification of wave activity that produces long waves, which in turn penetrate almost to the bottom. The strong mixing generated from the wave-induced turbulence leads to the entrainment of cool waters from the bottom and subsequent cooling of the sea surface.

The in situ observations indicate that the maximum poststorm SST cooling is approximately 3.5°C at all locations except at buoy 42041 where the observed SST cools by only 1.6°C. Both 42041 and 42001 are located within the northern warm-core-ring and are expected to reduce the SST cooling during the passage of the hurricane. The observations reveal that there is considerably less cooling in the northern (42041) part of the

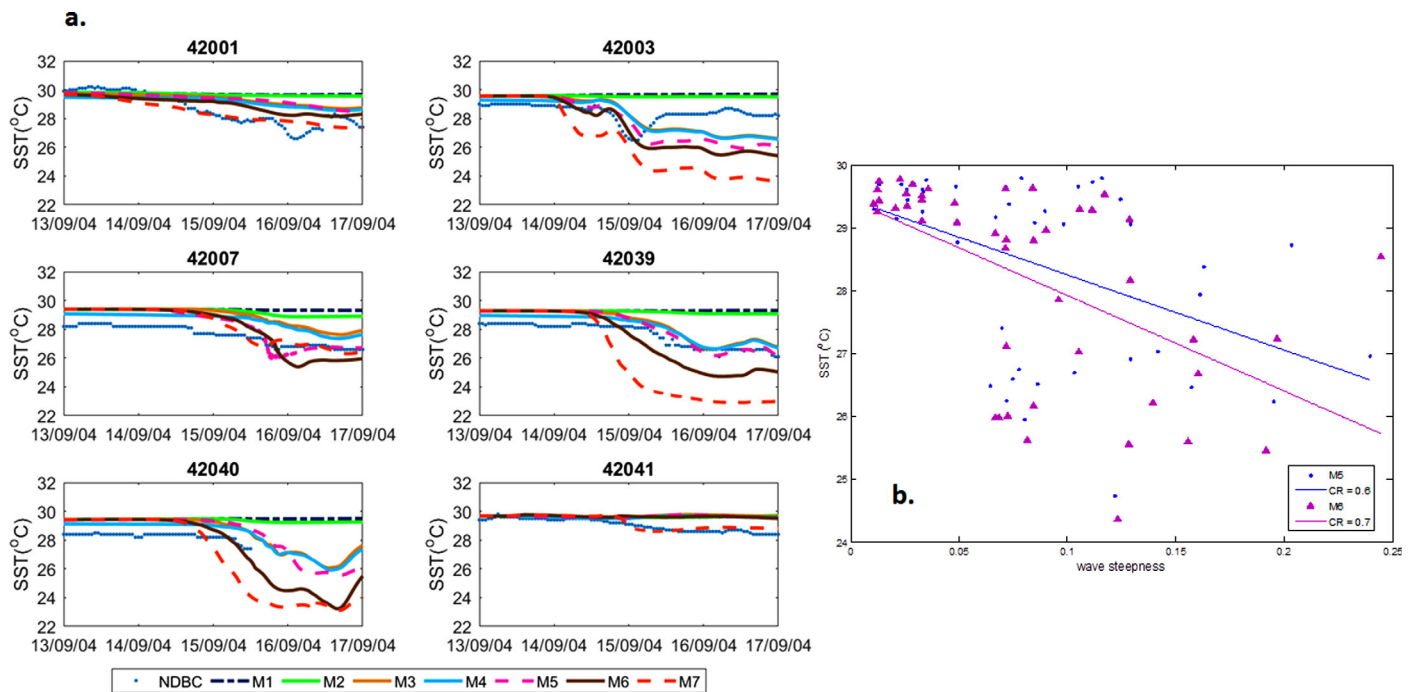


Figure 5. (a) Observed (in situ) SST and modeled SST for numerical experiments M1 to M7—showing the impacts of various vertical mixing processes. (b) Correlation of modeled SST (°C) with model-derived wave steepness ($kH_s/2$) for M5 (blue), and M6 (pink).

ring than in the southern part (42001), where the modeled wind stress is higher. The modeled current and wind vectors are nearly in opposite directions at both locations (Figure 4b), however, at the northern location (42041), the modeled wind stress is weaker and therefore does not contribute significantly to the production of turbulence in comparison with the southern location (42001), therefore leading to less mixing.

At location 42003, where there is a strong modeled eastward current present (Figure 4b), the recorded in situ SST drops by nearly 3°C after the passage of the hurricane but quickly recovers within 6–8 h by 2°C (Figure 4a). The model captures the poststorm cooling with good accuracy but is unable to reproduce the recovery. This again can be attributed to the presence of the mesoscale features and the accuracy of their locations in the model initialization process. The coupled atmosphere-ocean-wave model developed by Zambon *et al.* [2014] for Hurricane Ivan exhibited similar trend in the predicted SST and was not successful in reproducing the warming of the SST at buoy 42003 following the rapid cooling. Their model produced a larger cooling bias of nearly 2.5°C at this location, which they attributed to the inclusion of wave fields and large wind stress. Unlike our study, their model was dynamically coupled and included feedback from the atmospheric model, suggesting that the structure of the hurricane winds or the lack of feedback from the atmosphere may not be the reason our model was not able to reproduce the increase in SST following the passage of the storm at location 42003.

From the above discussion, it is apparent that the location of the warm-core-rings will have a strong effect on the SST and hence on the model’s ability to reproduce it. Although the rigorous initialization process defines the location and strength of the mesoscale features with reasonable accuracy based on satellite observations and reanalysis data, the locations (or magnitudes) of the features may not be precise enough, leading to errors in the model predictions of SST.

An interesting feature of the model is that it generally underestimates the SST cooling at buoys that are located on the right-hand side (RHS) of the storm track, which is the side where wind stress is stronger, while SST cooling on the weaker left-hand side (LHS) is overestimated. The right side of the hurricane has resonant wind and current rotations [Sanford *et al.*, 2011; Price, 1981] in addition to resonance between the wind and the storm translation—these result in larger waves [Young, 2003; Moon *et al.*, 2003], a corresponding increase in turbulence, and therefore enhanced cooling on the RHS. We believe that the warming and

cooling associated with the existence of the Loop currents and the associated eddies may be one reason for this behavior while another distinct possibility is the impact of the nonbreaking wave-induced mixing.

Figure 4c presents a comparison of the model and recorded temperatures near the seabed. The near-bottom temperatures have been taken from *Teague et al.* [2007], who analyzed data collected from an array of 14 acoustic Doppler current profilers (ADCP) deployed along the outer continental shelf and upper slope in the north-eastern Gulf of Mexico. The ADCP data commences on 15 September 2004 and all 14 ADCPs were located in the vicinity of NDBC 42040. The model data have been extracted at the bottom layer at this location and compared with the two ADCPs that were located closest to 42040 [see *Teague et al.*, 2007, Figures 1 and 7]. We recognize that the depth of the model extraction point (42040) is shallower than the depths at the two ADCP locations; however, the primary purpose of the comparison is to provide an indicative model skill in reproducing temperatures below the sea surface. Both the model and the ADCP show that the near-bottom temperatures varied between 8 and 11°C between 15 and 17 September 2004. A semiquantitative comparison between the measured and modeled currents was undertaken where the model peak currents were extracted near the measurement sites. The measured peak currents were between 125 and 168 cm/s on the slope locations and were directed westward to north-westward in the upper 50 m of the water column [*Teague et al.*, 2007]. In comparison, the corresponding model currents were 150 cm/s directed northwest. Although a detailed validation has not been performed for the predicted currents because of the limited current observations, the model generally reproduces the current speeds and directions with reasonable accuracy.

4.2. Effects of the Nonbreaking Wave Parameterization

The results of the experiments M1–M7 are presented in Figure 5a. As expected, the SST for M1 remains constant at all locations as all major processes responsible for vertical mixing have been made negligible. This was achieved by assigning extremely small values to the wind stress and the vertical turbulent kinetic energy; by omission of the nonbreaking wave parameterization; and by excluding the dynamic ocean coupling with waves. Inclusion of the turbulent kinetic energy with minimal wind stress (M2) leads to very minor cooling of the SST with the only discernible cooling effects evident at the shallow water location of buoy 42007. The addition of the wind stress in M3 leads to a dramatic cooling of the SST of up to 3.5°C thus confirming that the strong wind forcing is a major source of turbulence that leads to the mixing and cooling of the upper ocean layers. In this case, the wind forcing generates ocean surface currents and vertical current shear, which in turn produces the turbulence.

Including the nonbreaking wave parameterization without the dynamic coupling of waves (M4), that is, assuming spatially and temporally uniform waves ($H_s = 2$ m, wave number = 0.01), leads to only a marginal reduction in the modeled SST. While the currents are generated by the hurricane wind forcing, the uniform wave conditions do not represent typical storm waves in a hurricane, which may exceed 10 or 20 m in height. Application of constant extreme values of H_s all over the entire model domain would result in the high values of H_s away from the high wind stress areas. This would be highly unrealistic, therefore an average value of H_s of 2 m for M4 was chosen. The turbulence generated by the vertical shear of the cyclonic currents is substantially larger relative to the turbulence created by the nonbreaking wave-induced mixing from noncyclonic waves in this case. Consequently, the addition of the nonbreaking wave parameterization does not contribute to significant additional cooling of the modeled SST in M4.

In the model experiment M5, MIPOM-TC is dynamically coupled to the wave model, WW3. The hurricane wind forcing was applied to both the ocean and wave models and variables of sea surface height, currents, and wave parameters were exchanged between the models. However, the effects of nonbreaking waves on the vertical mixing were not included. The effects of the turbulence generated by the growing and decaying wave fields and their interaction with the currents leads to an SST cooling of approximately 1°C at 42003 and nearly 3.5°C at 42040, which is located at the center of the hurricane track and hence subject to intense wind and waves. The effect of waves on SST cooling at other locations is minor. On adding the nonbreaking wave-induced parameterization with $b_1 = 0.0014$ to the coupled model setup in M6, there is further SST cooling of up to 2°C mainly at 42039 and 42040 in the model. The model still underestimates the cooling at 42001, 42007, and 42041 relative to the observations while slightly overestimating at the other locations. Changing the value of b_1 from constant to a varying value that is wave steepness dependent

Table 2. Model Skill for SST Predictions

Location	M5			M6			M7		
	Bias	RMSE	CR	Bias	RMSE	CR	Bias	RMSE	CR
42001 (LHS)	-0.14	0.67	0.84	-0.02	0.55	0.87	0.24	0.38	0.93
42003 (RHS)	-0.35	0.74	0.79	-0.21	0.83	0.79	0.29	1.48	0.80
42007 (LHS)	-0.94	1.02	0.73	-0.94	0.99	0.84	-0.80	0.89	0.83
42039 (RHS)	-0.81	0.84	0.92	-0.53	0.81	0.89	0.06	1.74	0.83
42040 (Center)	-0.75	0.84	0.88	-0.55	0.76	0.92	-0.18	1.25	0.88
42041 (LHS)	-0.19	0.40	0.50	-0.18	0.37	0.77	-0.05	0.20	0.88

(M7) improves the model predictions at the three locations on the LHS of the track but makes them worse at the RHS of the track.

The effects of the nonbreaking wave parameterization on SST are further seen in the correlation of modeled SST with the model-derived wave steepness in M5 where there is no wave-induced mixing in comparison with M6 that includes wave-induced mixing (Figure 5b). The correlation coefficient for M6 is higher than that for M5 reflecting the influence of the nonbreaking wave mixing parameterization when included in the coupled ocean-wave model.

Overall, the model skill is improved by enhancing the turbulence due to nonbreaking waves (Table 2) either due to M6 or M7. Table 2 shows the mean bias, root-mean-square error (RMSE), and the correlation coefficient (CR) of the modeled SST (M5, M6, and M7) against the recorded SST at the six buoy locations. The mean bias for RHS of the cyclone track reduces by up to 0.3°C for M6. The reduction in RMSE for the same is modest at about 0.1°C. A reduction in bias and RMSE of approximately 0.2 for the LHS is achieved by M7. The CR shows an improvement of 0.1–0.2 from M5 to M6 or M7. At location 42041, the CR is increased by nearly 40% for M7.

The effects of the wave-induced parameterization using a b_1 scaled against wave steepness and a constant b_1 on 15 September 2004 1200 are presented in Figures 6a and 6b, respectively. On the strong side of the hurricane the modeled SST cools by 7°C when b_1 is scaled against the wave steepness (M7) and cools by 4°C with a constant b_1 (M6). On the weaker side, the modeled SST cooling is about 1–2°C for M7 and less than 1°C for M6. The cooling is noticeably suppressed in the areas where the warm-core rings are present as discussed earlier. The vorticity associated with the mesoscale features can distort the wind-driven upwelling, which is a major contributor to SST cooling [Jaimes and Shay, 2009]. Halliwell et al. [2011] report similar SST cooling on the strong side of the hurricane in their modeling exercise of Hurricane Ivan and speculated that it could be from an initial cooling bias in the model initialization, though they also considered the vertical mixing parameterizations as a possibility for the additional cooling.

The biggest contribution to mixing from the nonbreaking wave parameterization is clearly on the strong side of the hurricane where the peak waves are stronger and longer, and the turbulence due to wave-orbital motion is injected into the upper ocean layers. Figure 7 shows that the area where the modeled wavelengths are longer (greater than 300 m) in the right-rear quadrant is coincident with the area of the highest modeled SST cooling in Figure 6. The b_1 (in M7) ranges from 0.05 to 0.25 and directly responds to the modeled high wind stress and strong waves. The P_w at middepth is strongest in the rear right quadrant of the hurricane (Figure 7, bottom right).

We further analyze the impacts of nonbreaking wave parameterization on the temperature profiles. Longitudinal profiles of temperature predicted by model experiments M7 (Figure 8) and M6 (Figure 9) have been extracted along the storm track and perpendicular to the storm track (shown by the blue and green lines respectively in Figure 6). The differences in temperature profiles between M7 and M5 are presented in Figures 8b and 8d. The cooling effects of the nonbreaking wave-induced mixing extend approximately to a depth of 50 m (Figure 8b) below the surface on either side of the track; and extend to 100 m depth below the surface along the track (Figure 8d).

There is rapid cooling in the upper 50–100 m followed by an increase of temperature of about 2–4°C further below. The intensity of the surface cooling gradually decreases along the longitude from the east to the west consistent with the gradual weakening of the cyclone intensity from the east to the west. The patterns

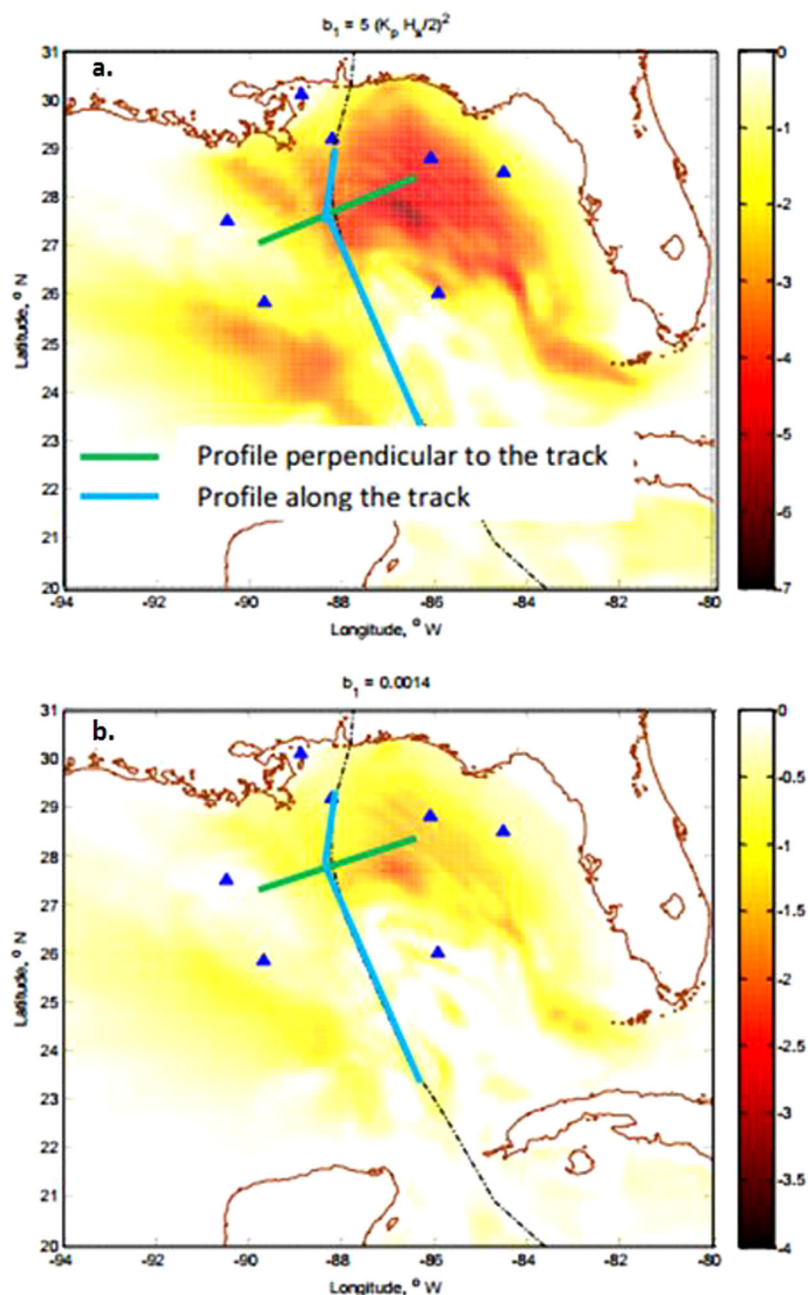


Figure 6. (a) Difference in SST between (top) M7 and M5 (M7 minus M5). (b) Difference in SST between (bottom) M6 and M5 (M6 minus M5) on 15 September 2004 1200. Increasing negative scale indicates increased SST cooling ($^{\circ}\text{C}$). The blue and green lines show the cross sections for longitudinal profiles.

for the differences in temperature between M6 and M5 (Figure 9) are similar to those in Figure 8 except the cooling by M6 is less dramatic in comparison with M7.

The modeled temperature profiles at each of the buoy locations (Figure 10) demonstrate the effects of the nonbreaking wave parameterization on the mixed layer depths. The mixed layer depth is defined as the depth where the temperature difference at that depth and the SST exceeds 0.5°C . We can see the progressive increase in mixed layer depths from M1 and M2 (no wind stress) to M3 and M4 (no dynamic coupling with waves), M5 (no wave-induced mixing), and M6 and M7 (with wave-induced mixing) at nearly all locations, in particular at the shallow water locations 42007, 42039, and 42040.

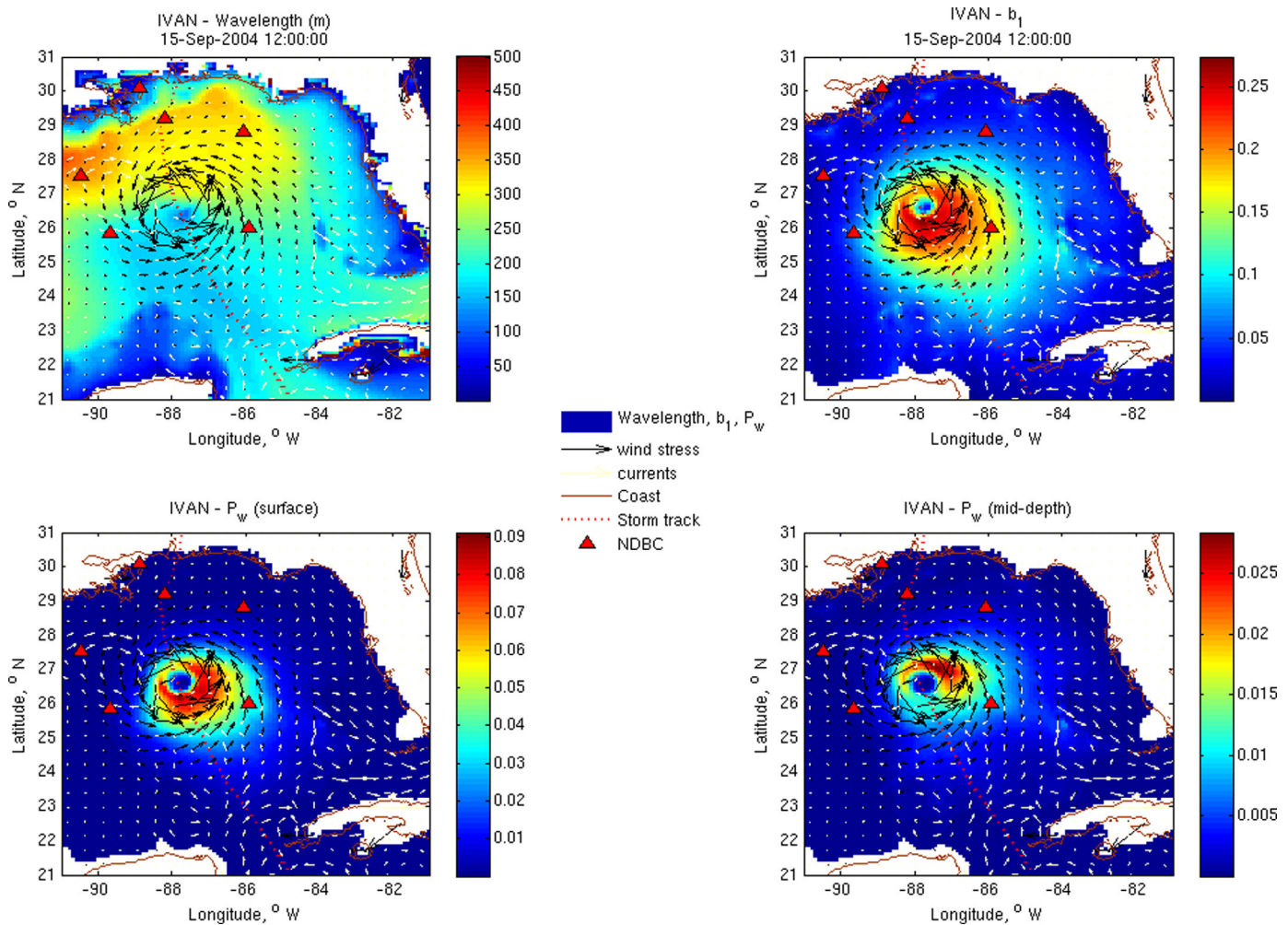


Figure 7. (top left) Wavelength; (top right) variability of $b_1 = 5 \left(\frac{H}{L}\right)^2$ in Exp. M7; (bottom left) turbulence production due to nonbreaking waves (P_w) at the surface; and (bottom right) P_w at middepth on 15 September 2004 1200 during Hurricane Ivan.

Location 42041 shows the least change in mixed layer depth between experiments M1 and M6, however, there is an increase of nearly 20 m between M5 and M7. This buoy is located on the weak side of the storm track and within the warm-core ring. Here the wind stress and the waves are small but the nonbreaking waves (with steepness-dependent b_1) generate sufficient turbulence to increase the mixed layer depth. The mixed layer depths at the deep locations (depths exceeding 1000 m) extend to depths exceeding 100 m (42001 and 42003 in Figure 10). The experiment M7 with the steepness-dependent wave parameterization predicts an increase of 20–25 m in the mixed layer depth relative to M5 (no wave-induced mixing) on the weak side (buoys 42001 and 42041) of the cyclone. On the stronger side of the hurricane, the difference in mixed layer depths between the models with no wave-induced mixing (M5) and those with wave-induced mixing with a constant b_1 (M6) is 42 m at buoy 42003 and 15 m at buoy 42039.

With waves with wavelengths ranging between 40 and 450 m during the passage of Hurricane Ivan, the longer waves inject enough turbulence into the water column that leads to the deepening of the mixed layer, entrainment of cooler waters from below the thermocline and ultimately to the cooling of SST.

Figure 11a shows the temporal evolution and the spatial variability of H_s during the passage of Hurricane Ivan as it progressed from the Caribbean Sea through the Gulf of Mexico. The peak H_s reached up to 20 m in response to the hurricane wind forcing with wind speeds exceeding 70 m/s. Given the reasonable agreement of the predicted H_s with the observed H_s at the NDBC buoys and the buoy at 42040 (center of the

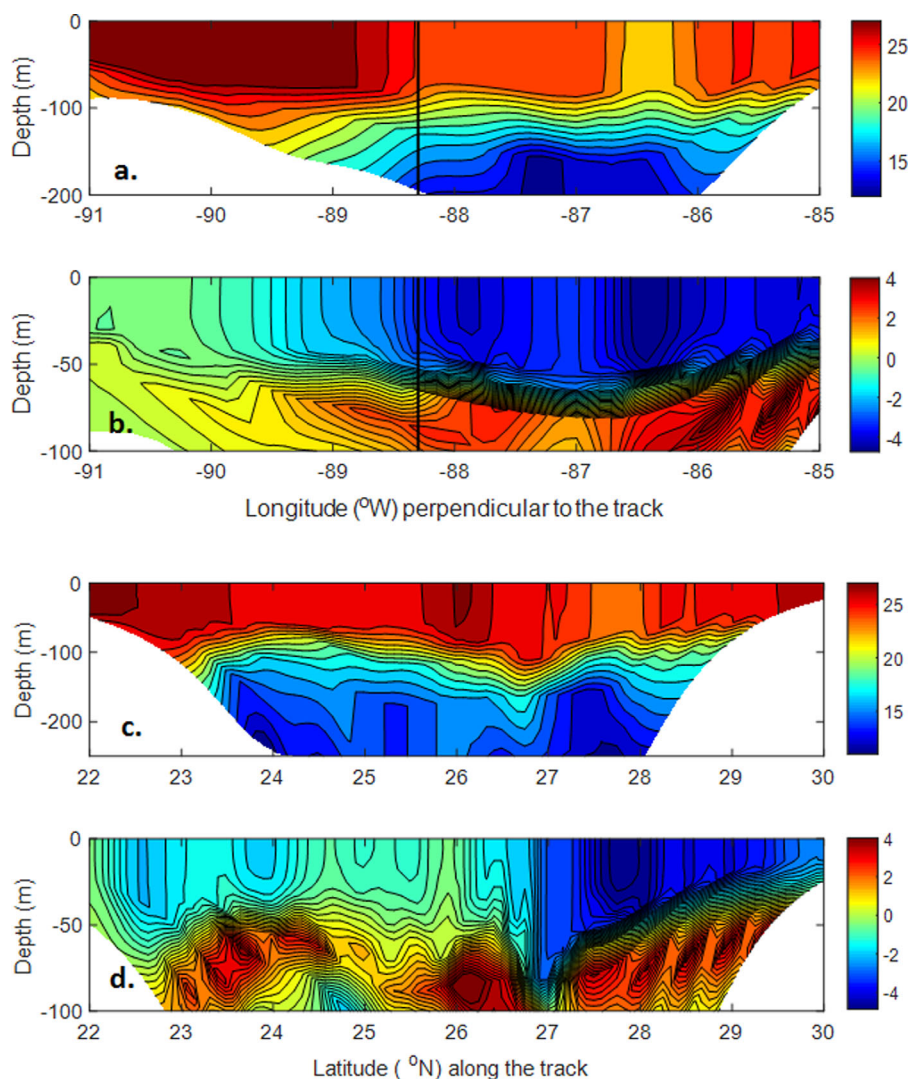


Figure 8. (a) Longitudinal profiles perpendicular to the track and along the track on 15 September 2004 1200. (a) Modeled temperature profile for M7 perpendicular to the track; (b) difference (M7 minus M5) in temperature between M7 and M5 perpendicular to the track; Solid black line indicates the track position; (c) model temperature profile along the track; (d) Difference (M7 minus M5) in temperature between M7 and M5 along the track. The legend represents the temperature scale in °C.

storm track) reaching H_s of 16 m before going adrift, the predicted peak H_s of 20 m in the right-hand quadrant of the hurricane should be realistic. The increased wave intensity leads to a larger production of turbulence via (1), and subsequently enhances the mixing via (4) and (5).

The wave field is further affected by refraction due to the spatially varying currents via (6). In an area where wind, wave, and current vectors are aligned, there is a reduction in wave energy, and when there is misalignment between the wave and current vectors the wave energy will increase [Fan *et al.*, 2009b]. Therefore, on the RHS of the storm, where the wave field is more developed, the currents result in a reduction of H_s . Fan *et al.* [2010] also investigated the effect of the translational speed of a moving TC on the momentum flux budget due to waves. They found that while the maximum reduction of the momentum flux along the radius of maximum winds is similar for translational speeds of 5 and 10 m/s, the wave effect on the momentum flux budget is enhanced by a moving TC relative to a stationary TC.

The effects of wind-wave interaction at the air-sea interface in tropical cyclones are discussed in detail by Fan *et al.* [2009a, 2009b] through the examination of the momentum fluxes in coupled ocean and wave models. From the analysis of the wave action equation, the study found that the wave field was mostly modulated by the horizontal gradient of the currents and the horizontal current advection of the waves. As

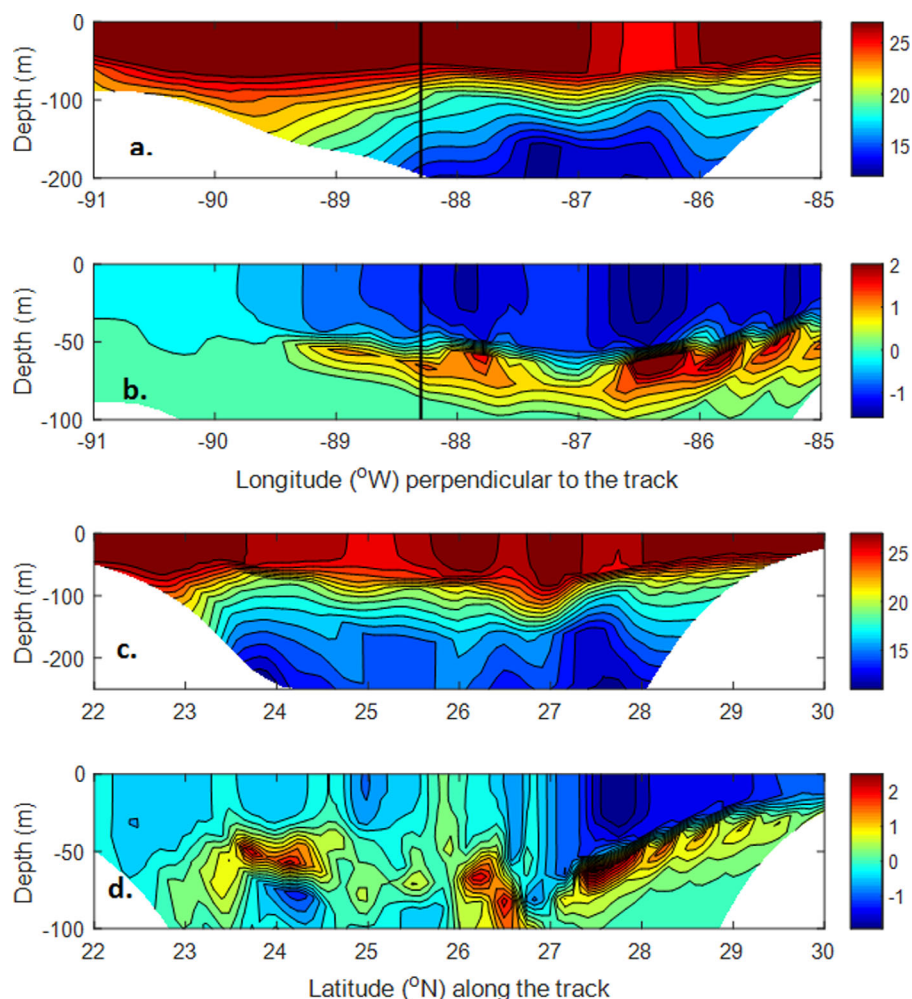


Figure 9. Same as in Figure 8 except M6 (M6 minus M5).

Hurricane Ivan passed over the Loop current and the warm and cold-core rings, the waves and currents were further modulated by the nonlinear wave-current interactions between the preexisting strong currents and the hurricane-generated waves and currents [Fan *et al.*, 2009b].

The SST cooling along the hurricane track during its passage from the Caribbean into the Gulf of Mexico is presented in Figure 12. The model predicts SST cooling of up to 7°C on the stronger side of the cyclone. Both the model and the in situ buoy observations indicate that the maximum SST cooling lags behind the peak H_s by about 6–12 h. The waves and currents respond to the hurricane wind forcing immediately while the dissipation of wave energy and the turbulence-generation mechanisms responsible for entraining the cooler waters from below the thermocline take some time for the warmer subsurface layer to mix with the cooler waters. Toffoli *et al.* [2012] report similar time lags of 10–20 h between the observed mixed layer depths and those calculated using wave-induced turbulence. Their study demonstrates that under the effect of TCs, the mixed layer depth deepens at an average speed of the order of 10^{-3} m/s, which would lead to a deepening of 50 m in about 10 h (or 3600 dominant wave periods). The observations of mixed layer depths indicate that the nonbreaking wave turbulence may have a major impact only when its contribution is much larger than the contribution from the shear currents, for example, through intensification of wave activity during TCs.

The predicted SST patterns (Figures 12a and 12b) are similar to the modeled SST and the blended SST patterns from satellite data presented in Halliwell *et al.* [2011] and Zambon *et al.* [2014]. The modeled SST from this study have also been compared against the Group for High Resolution Sea Surface Temperature (GHRSSST) Level 4 SST analysis (Figure 12b) that consists of SST observations from several instruments

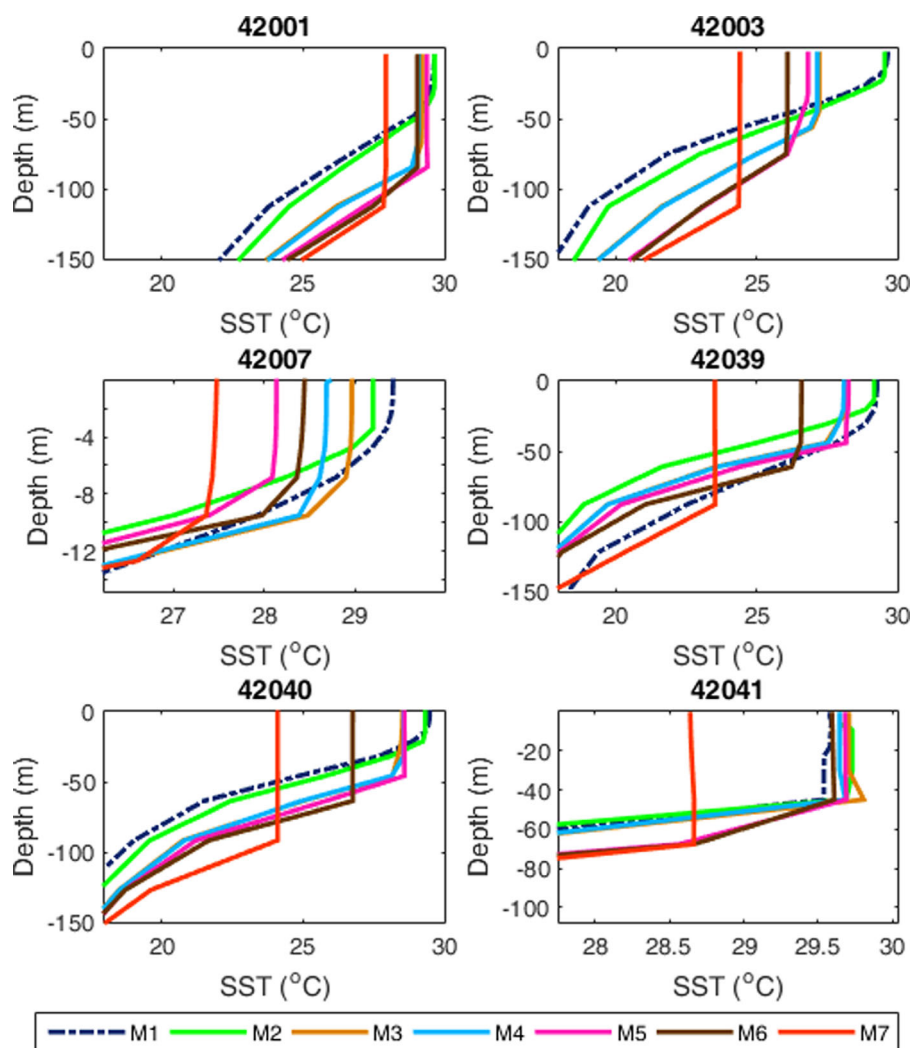


Figure 10. Vertical temperature profiles from numerical experiments M1–M7 extracted on 16 September 2004 00:00.

including the NASA Advanced Microwave Scanning Radiometer-EOS [AMSRE]; the Moderate Resolution Imaging Spectroradiometer [MODIS] on the NASA Aqua; and Terra platforms; the U.S. Navy microwave WindSat radiometer; and in situ SST observations from the NOAA iQuam project. The GHRSSST data are available as a single global data set for each day. The data for 16 September 2004 were downloaded from the NOAA/JPL website. The model data were averaged between 15 September 2004 0000 and 17 September 2004 to correspond with the daily GHRSSST. The model shows moderate degrees of similarities with the GHRSSST SST analysis. Both data sets show SST cooling of about 25°C in the northern Gulf of Mexico and 26–27°C in the Caribbean Sea. The model tends to overestimate the SST cooling, which was also seen in comparisons against in situ buoy data. This may be attributed to the overmixing by the model; the accuracy of the initialization of the Loop current and its eddies; warm-core and cold-core rings; the accuracy of the best track; and the accuracy of the interpolated wind fields.

To further test and validate the nonbreaking wave parameterization, in particular the impacts of the parameter b_1 on either side of the storm track in a different global region, we carried out a preliminary test simulation of TC Olwyn, a category 3 tropical cyclone in the Southern Hemisphere over Australia’s North West (NW) shelf. Another motivation for undertaking this test was that the NW Australian region is a highly active region for TC genesis and also has a large number of offshore oil and gas platforms. Any improvements in TC predictions would assist the offshore industry in mitigating safety risks and increasing efficiency. The b_1 computed for TC Olwyn showed a similar pattern to that of Hurricane Ivan with more mixing on the strong

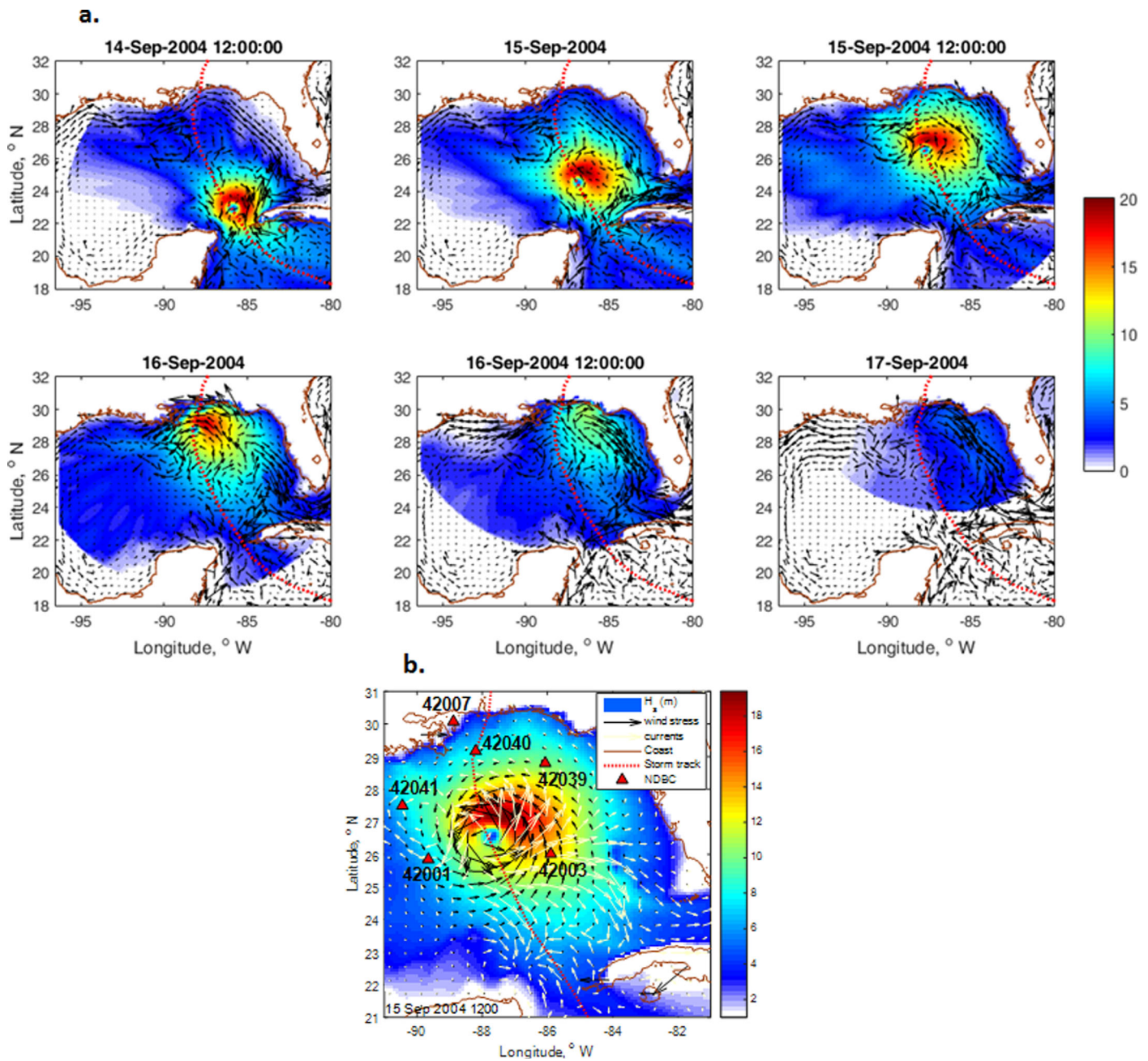


Figure 11. (a) Temporal and spatial evolution of H_s (m) (contours) for M6. Current vectors are shown in black. The red dotted line indicates the Hurricane Ivan track. (b) Wind stress (black), current velocity (white) vectors, and H_s contours for M7 on 15 September 2004 12:00.

side of the storm than the weak side. A brief summary of the coupled MIPOM-TC-WW3 modeling of TC Olwyn is included in Appendix A.

5. Summary and Conclusions

We have evaluated the ocean response to a new wave-induced turbulence parameterization under tropical cyclones settings. Unlike previous similar studies that include only surface wave-breaking or a wave-induced viscosity, the new wave parameterization does not rely on wave-breaking and is therefore independent of the wind stress. Another significant feature of the new wave parameterization is that it is added

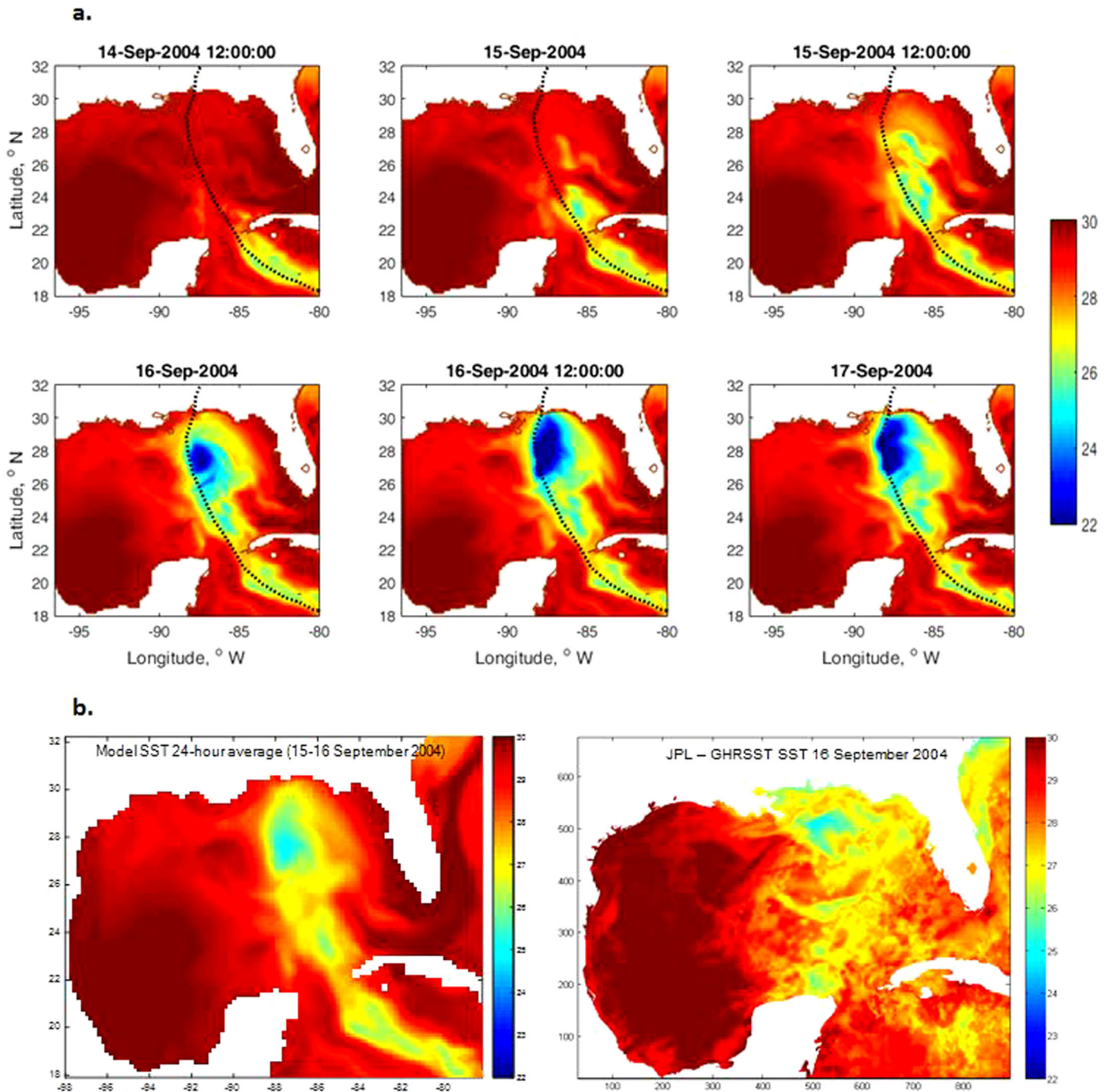


Figure 12. (a) Temporal and spatial evolution of model SST (°C) for M6. Black dotted line indicates the Hurricane Ivan track. (b) Comparison of model SST (°C) (left) with the Group for High Resolution Sea Surface Temperature (GHRSSST) Level 4 SST analysis produced as a retrospective data set (4 day latency) at (right) the JPL Physical Oceanography. Source: <http://podaac.jpl.nasa.gov/datasetlist?ids=&values=&search=GHRSSST&view=list>.

directly to the turbulence production terms in the standard Mellor-Yamada turbulence model, thus avoiding the issues that can arise from adding turbulent viscosities.

We have shown that the nonbreaking wave-induced turbulence leads to improved predictions of SST cooling due to the enhanced mixing that penetrates deeper (of the order of the length scale of wave lengths) in the water column. Accurate predictions of SST are essential in tropical cyclone modeling where the cyclone genesis and strength are highly dependent on SST heating and cooling.

We employed the new MPI version of POM (MPIPOM-TC) for testing and validating the new parameterization for nonbreaking wave-induced turbulence. We compared it against various formulations that parameterize the different physical processes of vertical mixing in the ocean. The ocean-circulation model MPIPOM-TC was dynamically coupled to the surface wave model WW3, and both models were forced by the atmospheric hurricane wind forcing. The wave-induced parameterization was introduced into the ocean model and the wave-current interactions were accounted for in the wave model. The model results were compared with field observations of the surface waves and SST from the NDBC buoy time series during Hurricane Ivan. Assuming that the NDBC provided reliable observations, we found that the agreement between the modeled and in situ H_s was generally good. There were some model errors in timing at one location and slight overestimation at the site located within the warm-core ring. Since the wave fields are directly influenced by the wind fields and the storm propagation speed, we believe that an improvement in the estimation of both the wind profiles and the storm track and propagation speed would lead to better model performance.

The inclusion of the nonbreaking wave parameterization in the model was found to significantly improve the model performance on the weaker side of the cyclone while the improvement on the strong side of the cyclone was marginal. We determined the influence of the parameter b_1 in enhancing the SST cooling and increasing the mixed layer depth. Using a constant value of b_1 (0.0014) provided good agreement with the observed SST on the strong side of the hurricane while a wave-steepness-dependent b_1 resulted in a better match with the in situ data on the weaker side of the hurricane. The behavior of b_1 in relation to the weaker and stronger sides of the hurricane was further examined in simulations of tropical cyclone Olwyn over north-west Australia, where in situ measurements were available on the strong side of the tropical cyclone. Similar to Hurricane Ivan, the model using a constant value of b_1 was found to be closer to the SST observations than the model with steepness-dependent b_1 .

As with any numerical modeling study, we acknowledge that the model results from our study are subject to uncertainties associated with the various parameterizations of the model physics, initial conditions, grid resolution, and biases due to the lack of dynamic atmosphere coupling. The accuracy of the storm track and consequently the accuracy of the forcing wind fields will have a major influence on the model outcomes. The dynamic atmospheric coupling along with the secondary effects of heat flux and short-wave radiation will be investigated in future studies. The diagnostics of various parameterizations that represent the physical processes in the atmosphere, ocean, and the wave models and the atmosphere-ocean-waves interactions are complex and require further in-depth research and analysis.

Appendix A: TC Olwyn

TC Olwyn generated wind speeds exceeding 43 m/s and caused extensive damage along the NW Australian coast as it made landfall on 14 March 2015. The TC passed directly over a permanent measurement site (North Rankin A) in water depth of 125 m, where Woodside Energy Ltd. has been collecting data for the past three decades [Toffoli *et al.*, 2012]. A new grid and bathymetry for the Southern Hemisphere was set up

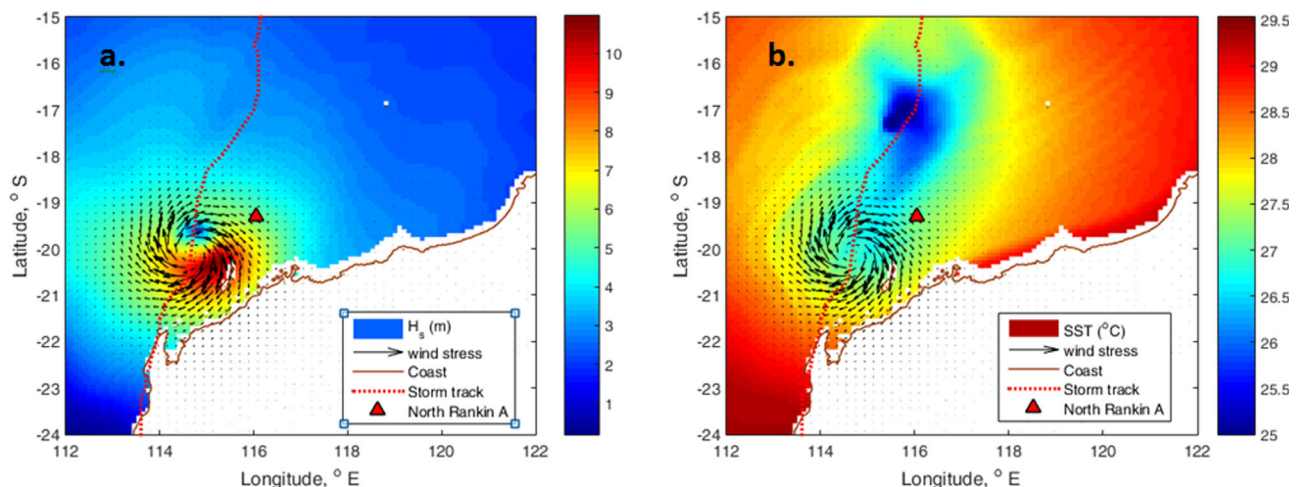


Figure A1. (a) (left) Wind stress vectors and H_s (m) contours; (b) (right) SST contours on 12 March 2015 0900. TC Olwyn track is indicated by the red dashed line.

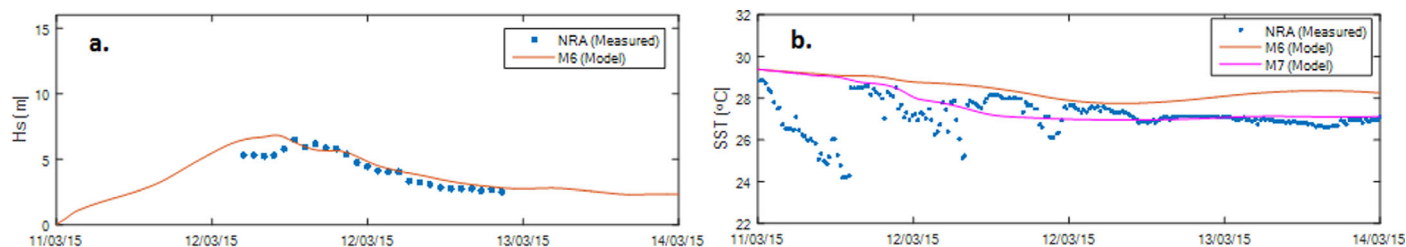


Figure A2. (a) (top) Time series of measured and modeled H_s (m); (b) (bottom) SST at the measurement station (NRA). Please note that the recorded temperature at 10 m below the sea surface has been considered representative of the SST.

and simulations corresponding to M5, M6, and M7 (Table 1) were conducted. Our preliminary model setup did not include the background Leeuwin Current. The modeled fields of wind, waves, SST, and the time series of H_s and SST are presented in Figures A1 and A2. The model predicts a peak H_s exceeding 11 m within the TC core (Figure A1a) as the cyclone moves from the north to the south. The SST cooling of 5–6°C occurs following the passage of the TC Olwyn (Figure A2b). The model H_s compares well with the recorded H_s (Figure A2a). As seen for Hurricane Ivan, the H_s attained a maximum value in quick response to the strong wind forcing while the maximum SST cooling lagged by 10–15 h. The observed temperature time series shows oscillations with periods between 11 and 13 h (Figure A2b) due to the presence of strong internal wave activity [Toffoli et al., 2012].

Figure A2b shows that the model (M7) with steepness-dependent b_1 overestimates the cooling when compared to the model (M6) with a constant b_1 of 0.0014. This is consistent with the results for Hurricane Ivan where a constant b_1 was shown to have a better match with the observed SST on the strong side of the cyclone. In situ observations were available only on the strong side of the TC Olwyn. Future studies will include the simulation of cyclones that have passed on either side of the measurement site to further evaluate the effects of the nonbreaking wave parameterization.

Acknowledgments

The authors gratefully acknowledge funding for this study from the Australian Research Council Discovery grant DP130100227 and the U.S. Office of Naval Research grant N00014-13-1-0278. The TC Olwyn data were provided by Woodside Energy Ltd. The manuscript greatly benefited from the comments provided by Jasper Wijnands of the University of Melbourne, and by the anonymous reviewers. The simulations were performed on the gSTAR National facility at the Swinburne University of Technology. gSTAR is funded by the Swinburne and the Australian Government's Education Investment Fund. All data presented in this paper have been referenced in figures, tables, text, and references. Satellite data has been sourced from <http://podaac.jpl.nasa.gov/datasetlist?ids=&values=&search=GHRSS&view=list>.

References

- Agrawal, Y. C., E. A. Terray, M. A. Donelan, P. A. Hwang, A. J. Williams III, W. M. Drennan, K. K. Kahma, and S. A. Krtagorodskii (1992), Enhanced dissipation of kinetic energy beneath surface waves, *Nature*, *359*, 219–220, doi:10.1038/359219a0.
- Arduin, F., B. Chapron, and F. Collard (2009), Observation of swell dissipation across oceans, *Geophys. Res. Lett.*, *36*, L06607, doi:10.1029/2008GL037030.
- Arduin, F., et al. (2010), Semiempirical dissipation source functions for ocean waves, Part I: Definition, calibration, and validation, *J. Phys. Oceanogr.*, *40*, 1917–1941.
- Babanin, A. V. (2006), On a wave-induced turbulence and a wave-mixed upper ocean layer, *Geophys. Res. Lett.*, *33*, L20605, doi:10.1029/2006GL027308.
- Babanin, A. V. (2011), *Breaking and Dissipation of Surface Ocean Waves*, 463 pp., Cambridge Univ. Press, Cambridge, U. K.
- Benilov, A. Y. (2012), On the turbulence generated by the potential surface waves, *J. Geophys. Res.*, *117*, C00J30, doi:10.1029/2012JC007948.
- Babanin, A. V., and D. Chalikov (2012), Numerical investigation of turbulence generation in non-breaking potential waves, *J. Geophys. Res.*, *117*, C00J17, doi:10.1029/2012JC007929.
- Babanin, A. V., and B. K. Haus (2009), On the existence of water turbulence induced by nonbreaking surface waves, *J. Phys. Oceanogr.*, *39*, 2675–2679.
- Blumberg, A. F., and G. L. Mellor (1987), A description of a three-dimensional coastal ocean circulation model, in *Three-Dimensional Coastal Ocean Models*, vol. 4, edited by N. Heaps, pp. 1–16, AGU, Washington, D. C.
- Bueti, M. R., I. Ginis, and M. L. Rothstein (2014), Tropical cyclone-induced thermocline warming and its regional global impacts, *J. Clim.*, *27*, 6978–6999.
- Chalikov, D., and V. Makin (1991), Models of the wave boundary layer, *Boundary Layer Meteorol.*, *56*, 83–89.
- Craig, P. D., and M. L. Banner (1994), Modeling wave-enhanced turbulence in the ocean surface layer, *J. Phys. Oceanogr.*, *24*, 2546–2559.
- Dai, F., F. Qiao, W. Sulisz, L. Han, and A. V. Babanin (2010), An experiment on the non-breaking surface-wave-induced vertical mixing, *J. Phys. Oceanogr.*, *40*(9), 2180–2188.
- Donelan, M. A., B. K. Haus, N. Reul, W. J. Plant, M. Stiassnie, H. C. Graber, O. B. Brown, and E. S. Saltzman (2004), On the limiting aerodynamic roughness of the ocean in very strong winds, *Geophys. Res. Lett.*, *31*, L18306, doi:10.1029/2004GL019460.
- ETOPO5 (1988), *Data Announcement 88-MGG-02 (1988), Digital relief of the Surface of the Earth*, NOAA, Natl. Geophys. Data Cent., Boulder, Colo.
- Fan, Y., I. Ginis, and T. Hara (2009a), The effect of wind-wave interactions on air-sea momentum fluxes and ocean response in tropical cyclones, *J. Phys. Oceanogr.*, *39*, 1019–1034, doi:10.1175/2008JPO4066.l.
- Fan, Y., I. Ginis, T. Hara, C. W. Wright, and E. J. Walsh (2009b), Numerical simulations and observations of surface wave fields under an extreme tropical cyclone, *J. Phys. Oceanogr.*, *39*, 2097–2116, doi:10.1175/2009JPO4224.l.
- Fan, Y., I. Ginis, and T. Hara (2010), Momentum flux budget across the air-sea interface under uniform and tropical cyclone winds, *J. Phys. Oceanogr.*, *40*, 2221–2242, doi:10.1175/2010JPO4299.l.
- Ghantous, M., and A. V. Babanin (2014a), Ocean mixing by wave orbital motion, *Acta Phys. Slovaca*, *64*, 1–56.

- Ghantous, M., and A. V. Babanin (2014b), One-dimensional modelling of upper ocean mixing by turbulence due to wave orbital motion, *Nonlinear Processes Geophys.*, *21*, 325–338.
- Halliwell, G. R., Jr., L. K. Shay, J. K. Brewster, and W. J. Teague (2011), Evaluation and sensitivity analysis of an ocean model response to Hurricane Ivan, *Mon. Weather Rev.*, *139*, 921–945, doi:10.1175/2010MWR3104.1.
- Holland, G. J. (1980), An analytic model of the wind and pressure profiles in hurricanes, *Mon. Weather Rev.*, *108*, 1212–1218, doi:10.1175/1520-0493(1980)108<1212:AAMOTW>2.0.CO;2.
- Holland, G. J., J. I. Belanger, and A. Fritz (2010), A revised model for radial profiles of hurricane winds, *Mon. Weather Rev.*, *138*(12), 4393, doi:10.1175/2010MWR3317.1.
- Huang, C., and F. Qiao (2010), Wave-turbulence interaction and its induced mixing in the upper ocean, *J. Geophys. Res.*, *115*, C04026, doi:10.1029/2009JC005853.
- Huang, C., F. Qiao, and Z. Song (2008), The effect of the wave-induced mixing on the upper ocean temperature in a climate model, *Acta Oceanol. Sin.*, *27*, 104–111.
- Huang, C., F. Qiao, Z. Song, and T. Ezer (2011), Improving simulations of the upper ocean by inclusion of surface waves in the Mellor–Yamada turbulence scheme, *J. Geophys. Res.*, *116*, C01007, doi:10.1029/2010JC006320.
- Jacobs, C. A. (1978), Numerical simulations of the natural variability in water temperature during BOMEX using alternative forms of the vertical eddy exchange coefficients, *J. Phys. Oceanogr.*, *8*, 119–141.
- Jaimes, B., and L. K. Shay (2009), Mixed layer cooling in mesoscale ocean eddies during Hurricane Katrina and Rita, *Mon. Weather Rev.*, *137*, 1320–1337.
- Janssen, P. A. E. M. (1989), Wave-induced stress and drag of air-flow over sea waves, *J. Phys. Oceanogr.*, *19*, 745–754.
- Kantha, L. H., and C. A. Clayson (2004), On the effect of surface gravity waves on mixing in the oceanic mixed layer, *Ocean Modell.*, *6*, 101–124.
- Li, Y., S. Peng, J. Wang, and J. Yan (2014), Impacts of nonbreaking wave-stirring-induced mixing on the upper ocean thermal structure and typhoon intensity in the South China Sea, *J. Geophys. Res. Oceans*, *119*, 5052–5070, doi:10.1002/2014JC009956.
- Mellor, G. L. (2004), Users guide for a three-dimensional, primitive equation, numerical ocean model, in *Program in Atmospheric and Oceanic Sciences*, 56 pp., Princeton Univ., Princeton, N. J.
- Mellor, G., and A. Blumberg (2004), Breaking and ocean surface layer thermal response, *J. Phys. Oceanogr.*, *4*, 693–698.
- Mellor, G. L., and T. Yamada (1982), Development of a turbulence closure model for geophysical fluid problems, *Rev. Geophys. Space Phys.*, *20*, 851–875, doi:10.1029/RG020i004p00851.
- Melville, W. K. (1994), Energy dissipation by breaking waves, *J. Phys. Oceanogr.*, *24*, 2014–2049.
- Moon, I., I. Ginis, T. Hara, H. L. Tolman, W. Wright, and E. J. Walsh (2003), Numerical simulations of sea surface directional wave spectra under hurricane wind forcing, *J. Phys. Oceanogr.*, *33*, 1680–1706, doi:10.1175/2410.1.
- Moon, I., I. Ginis, T. Hara, and H. L. Tolman (2004a), Effect of surface waves on air-sea momentum exchange: Part 1: Effect of mature and growing seas, *J. Atmos. Sci.*, *61*, 2321–2333.
- Moon, I., I. Ginis, T. Hara, and H. L. Tolman (2004b), Effect of surface waves on air-sea momentum exchange: Part 2: Behaviour of drag coefficient under tropical cyclones, *J. Atmos. Sci.*, *61*, 2321–2333.
- Moon, I., I. Ginis, T. Hara, and B. Thomas (2007), Physics-based parameterization of air sea momentum flux at high wind speeds and its impact on hurricane intensity predictions, *Mon. Weather Rev.*, *135*, 2869–2878.
- Moon, I., I. Ginis, and T. Hara (2008), Impact of reduced drag coefficient on ocean wave modelling under hurricane conditions, *Mon. Weather Rev.*, *136*, 1217–1223.
- Phillips, O. M. (1961), A note on the turbulence generated by gravity waves, *J. Geophys. Res.*, *66*(9), 2889–2893.
- Pleskachevsky, A., M. Dobrynin, A. V. Babanin, H. Günther, and E. Stanev (2011), Turbulent mixing due to surface waves indicated by remote sensing of suspended particulate matter and its implementation into coupled modeling of waves, turbulence and circulation, *J. Phys. Oceanogr.*, *41*, 708–724.
- Powell, M. D., P. J. Vickery, and T. A. Reinhold (2003), Reduced drag coefficient for high wind speeds in tropical cyclones, *Nature*, *422*, 279–283.
- Price, J. F. (1981), Upper ocean response to a hurricane, *J. Phys. Oceanogr.*, *11*, 153–175, doi:10.1175/1520-0485(1981)011<0153:UOR-TAH>2.0.CO;2.
- Qiao, F., Y. Yeli, Y. Yang, Q. Zheng, C. Xia, and J. Ma (2004), Wave induced mixing in the upper ocean: Distribution and application to a global ocean circulation model, *Geophys. Res. Lett.*, *31*, L11303, doi:10.1029/2004GL019824.
- Qiao, F., Y. Yuan, T. Ezer, C. Xia, Y. Yang, X. Lu, and Z. Song (2010), A three-dimensional surface wave-ocean circulation coupled model and its initial testing, *Ocean Dyn.*, *60*, 1339–1355, doi:10.1007/s10236-010-0326-y.
- Reichl, B. G., D. Wang, T. Hara, I. Ginis, and T. Kukulka (2016), Langmuir turbulence parameterisation in tropical cyclone conditions, *J. Phys. Oceanogr.*, *46*, 863–886, doi:10.1175/JPO-D-15-0106.1.
- Sanford, T. B., J. B. Price, and J. B. Girtton (2011), Upper-ocean-response to hurricane Frances (2004) observed by profiling EM-APEX floats, *J. Phys. Oceanogr.*, *41*, 1041–1056, doi:10.1175/2010JPO4313.1.
- Shu, Q., F. Qiao, Z. Song, and C. Xia (2011), Improvement of MOM4 by including surface wave-induced vertical mixing, *Ocean Modell.*, *40*, 42–51, doi:10.1016/j.ocemod.2011.07.005.
- Teague, W. J., M. J. Carron, and P. J. Hogan (1990), A comparison between the Generalized Digital Environmental Model and Levitus climatologies, *J. Geophys. Res.*, *95*(C5), 7167–7183, doi:10.1029/JC095iC05p07167.
- Teague, W. J., E. Jarosz, D. W. Wang, and D. A. Mitchell (2007), Observed oceanic response over the upper continental slope and outer shelf during Hurricane Ivan, *J. Phys. Oceanogr.*, *37*, 2181–2206.
- Thomson, J., M. S. Schwendeman, S. F. Zippel, S. Moghimi, J. Gemmrich, and W. E. Rogers (2016), Wave-breaking turbulence in the ocean surface layer, *J. Phys. Oceanogr.*, *46*, 1857–1869.
- Toffoli, A., J. McConochie, M. Ghantous, L. Loffredo, and A. V. Babanin (2012), The effect of wave-induced turbulence on the ocean mixed layer during tropical cyclones: Field observations on the Australian North-West Shelf, *J. Geophys. Res.*, *117*, C00J24, doi:10.1029/2011JC007780.
- Tolman, H. L. (2009), User manual and system documentation of WAVEWATCH III version 3.14, *Tech. Note 276*, NOAA/NWS/NCEP/EMC/MMAB, Camp Springs, Md.
- Tolman, H. L., and D. Chalikov (1996), Source terms in a third-generation wind wave model, *J. Phys. Oceanogr.*, *26*, 2497–2518.
- Walsh, K., A. V. Babanin, and L. Stoney (2015), Coupled ocean-atmosphere processes in tropical cyclones on short and long timescales, paper presented at CAWCR 9th Annual Workshop on Coupled Modelling and Prediction, Bureau of Meteorology, Melbourne, Australia.
- Wang, G., and F. Qiao (2008), Ocean temperature responses to Typhoon MSTs in the East China Sea, *Acta Oceanol. Sin.*, *27*, 26–38.

- Wang, Y., F. Qiao, G. Fang, and Z. Wei (2010), Application of wave-induced vertical mixing to the K profile parameterisation scheme, *J. Geophys. Res.*, *115*, C09014, doi:10.1029/2009JC005856.
- Yablonsky, R. M., and I. Ginis (2008), Improving the ocean initialization of coupled hurricane-ocean models using feature-based data assimilation, *Mon. Weather Rev.*, *136*, 2592–2607.
- Yablonsky, R. M., I. Ginis, B. Thomas, V. Tallapragada, D. Sheinin, and L. Bernardet (2015a), Description and analysis of the ocean component of NOAA's operational hurricane weather research and forecasting (HWRF) model, *J. Atmos. Oceanic Technol.*, *32*, 144–163.
- Yablonsky, R. M., I. Ginis, and B. Thomas (2015b), Ocean modelling with flexible initialization for improved coupled tropical cyclone-ocean model prediction, *Environ. Modell. Software*, *67*, 26–30, doi:10.1016/j.envsoft.2015.01.003.
- Young, I. R. (1988), Parametric hurricane wave prediction model, *J. Waterw. Port Coastal Ocean Eng.*, *114*, 637–652.
- Young, I. R. (2003), A review of the sea state generated by hurricanes, *Mar. Struct.*, *16*, 201–218.
- Young, I. R. (2006), Directional spectra of hurricane wind waves, *J. Geophys. Res.*, *111*, C08020, doi:10.1029/2006JC003540.
- Young, I. R., A. V. Babanin, and S. Zieger (2013), The decay rate of ocean swell observed by altimeter, *J. Phys. Oceanogr.*, *43*, 2322–2333.
- Zambon, J. B., R. He, and J. C. Warner (2014), Investigation of hurricane Ivan using the coupled ocean-atmosphere-wave-sediment transport (COAWST) model, *Ocean Dyn.*, *64*, 1535–1554, doi:10.1007/s10236-014-0777-7.
- Zieger, S., A. V. Babanin, and W. E. Rogers (2015), Observation-based source terms in the third-generation wave model WAVEWATCH, *Ocean Modell.*, *96*, 2–25, doi:10.1016/j.ocemod.2015.07.014.
- Zweers, N. C., V. K. Makin, J. W. de Vries, and G. Burgers (2010), A sea drag relation for hurricane wind speeds, *Geophys. Res. Lett.*, *37*, L21811, doi:10.1029/2010GL045002.